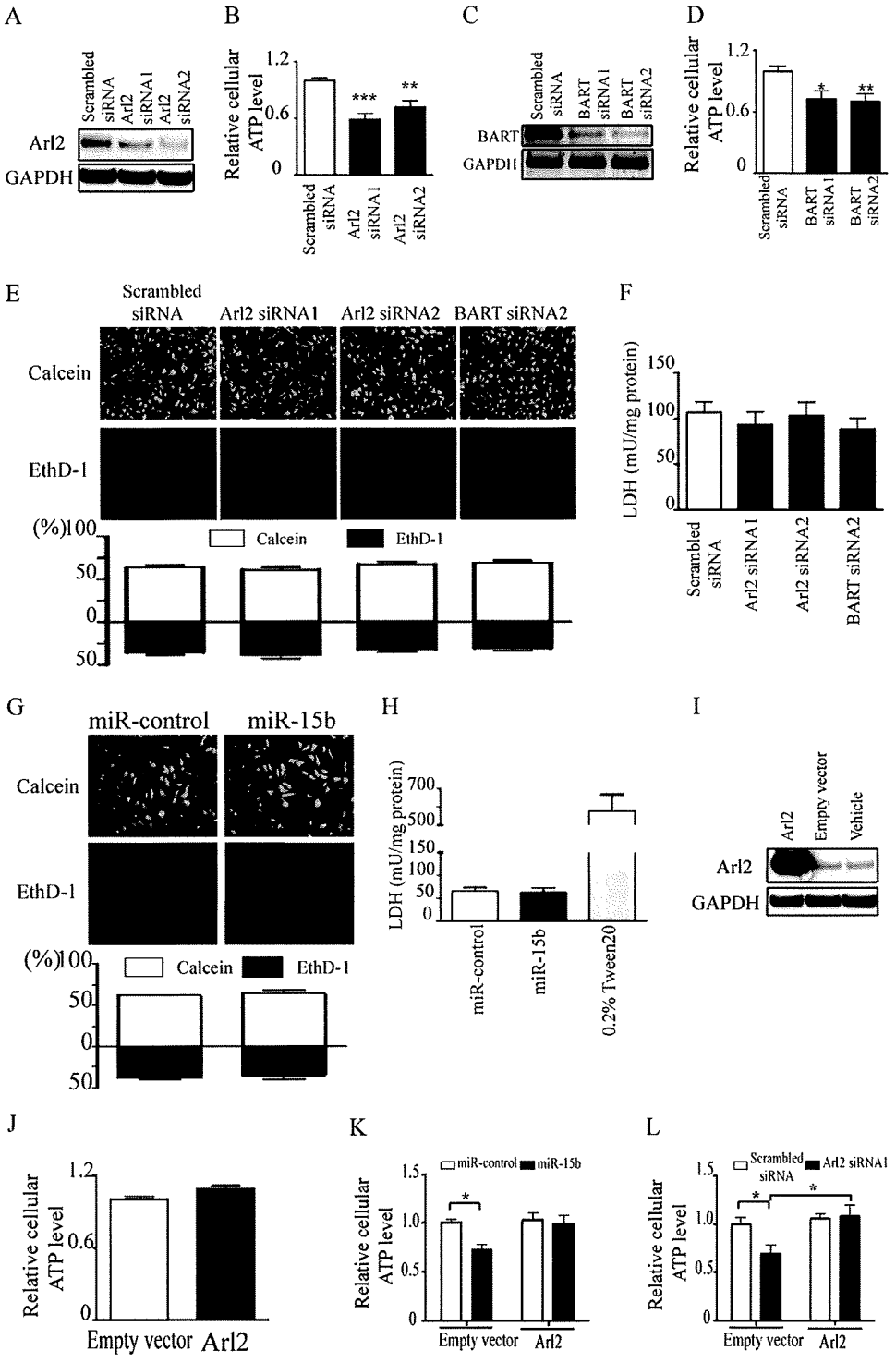

FIGURE 4. **Down-regulation of Arl2 decreases cellular ATP levels.** Assays were performed 72 h after transduction using a lentiviral vector in serum-containing medium. *A* and *B*, immunoblots of Arl2 (*A*) and cellular ATP levels (*B*) of NRVMs transduced with Arl2 siRNAs are shown. *C* and *D*, reverse transcription-PCR of BART (*C*) and cellular ATP levels (*D*) of NRVMs transduced with BART siRNAs are shown. In *B* and *D* data are presented as the mean ± S.E. of three independent experiments (*, $p < 0.05$; **, $p < 0.01$; ***, $p < 0.001$ *versus* scrambled siRNA). *E–H*, NRVMs stained by calcein AM (*green*) or ethidium homodimer (*red*) dyes (*E* and *G*) are shown. The bar graph indicates the proportions of live or dead cells. Lactate dehydrogenase (*LDH*) activity in the cultured medium was released from NRVMs (*F* and *H*). The values were standardized to the amounts of protein of the same samples. *I* and *J* show immunoblots of Arl2 (*I*) and cellular ATP levels (*J*) of NRVMs transduced with the Arl2 gene. *K* and *L*, cellular ATP levels were measured. NRVMs were co-transduced with either Arl2 gene, an empty vector, or vehicle along with miR-15b or miR-control (*K*) or along with either Arl2 siRNA1 or scrambled siRNA (*L*). The *bar graph* indicates values expressed as relative ATP levels compared with that with transduction with miR-control (*K*) or scrambled siRNA (*L*) along with an empty vector. Data are presented as the mean ± S.E. of four independent experiments (*, $p < 0.05$ *versus* control).

sequences in the proximal region, which is complementary to the seed sequence of miR-15b, was mutated to UGCUGGG (Fig. 2*B*). Cytomegalovirus-driven miR-15b, -16, -195, and -424 resulted in a decrease in luciferase activity, whereas similar amounts of miR-214 had no effect (Fig. 2*C*). Moreover, miR-15b, -16, -195, and -424 did not decrease the luciferase activities of mutated Arl2–3′-UTR constructs (Fig. 2*C*). The predicted binding site of miR-15b in the distal region of the Arl2 3′-UTR did not mediate gene suppression by miR-15b, -16, -195, and -424 (supplemental Fig. S4, *A* and *B*). miR-15b down-regulated both mRNA and protein of Arl2 (Fig. 2, *D* and *E*). These results indicated that miR-15b could target Arl2. A mixture of miR-15b, -16, -195, and -424 also decreased Arl2 mRNA and protein levels (Fig. 2, *D* and *E*) as well as cellular ATP levels to a similar extent as with miR-15b (Fig. 2*F*).

miR-15b, -16, -195, and -424 Have Similar Effects in the Recognition and Down-regulation of Arl2 mRNA—Although the seed sequences of miR-15b, -16, -195, and -424 are identical, the rest of the sequences are quite divergent. To test whether these miRNAs have an identical function in the regulation of Arl2, the dose-response effects of each of these miRNAs were examined. Cytomegalovirus-driven miR-15b, -16, -195, and -424 decreased the luciferase activities of Arl2 3′-UTR Luc constructs in a dose-dependent manner, and the degree of suppression was similar (Fig. 3*A*). Next, the effects of these miRNAs on Arl2 mRNA down-regulation were evaluated in 293FT cells. The transfection efficacy of miRNA expressing plasmids into 293FT cells was highest at a dose of 0.2 or 0.4 μg, at which Arl2 mRNA levels were maximally decreased to almost similar levels among miR-15b, -16, -195, and -424 (Fig. 3*C*). These results suggested that miR-15b, -16, -195, and -424 have similar effects in the recognition and down-regulation of Arl2 mRNA.

miR-15b Modulates ATP and Degenerates Mitochondria via Arl2

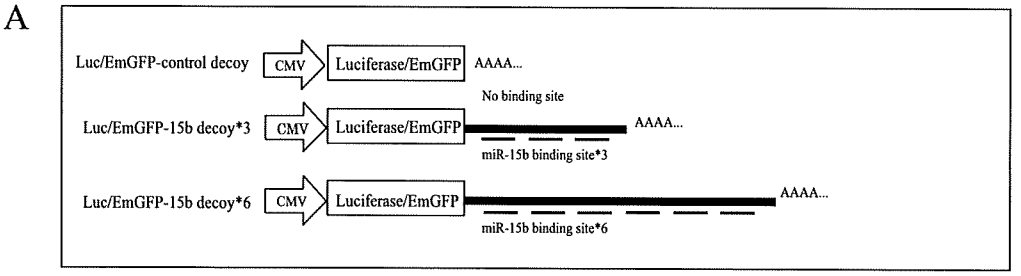

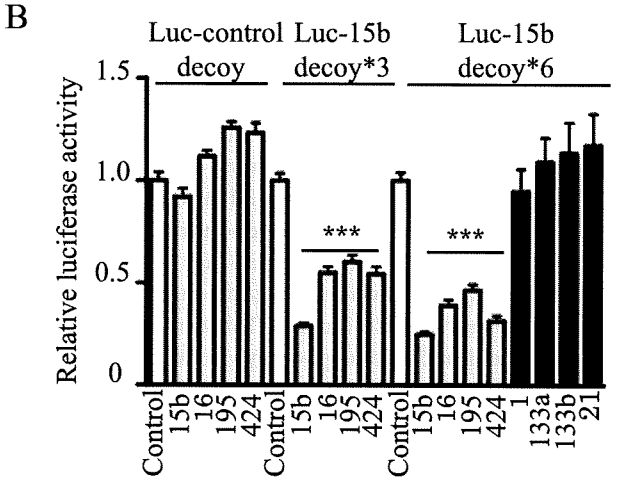

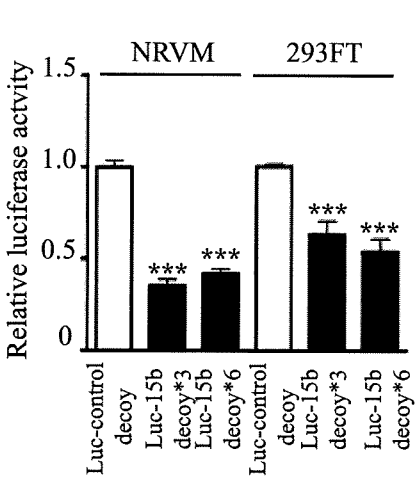

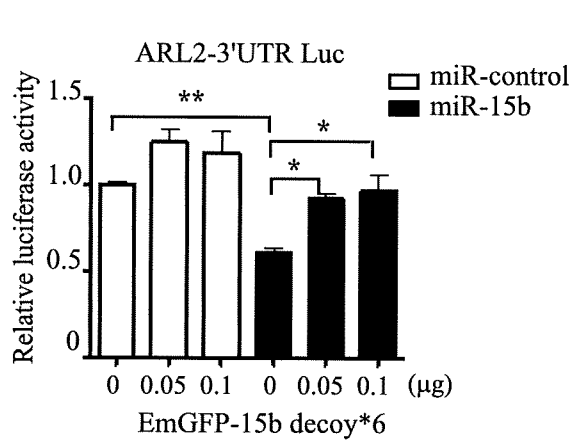

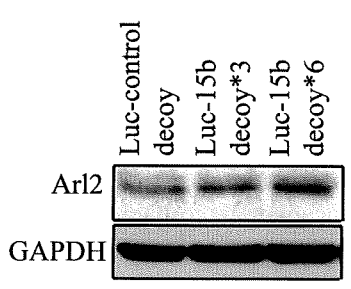

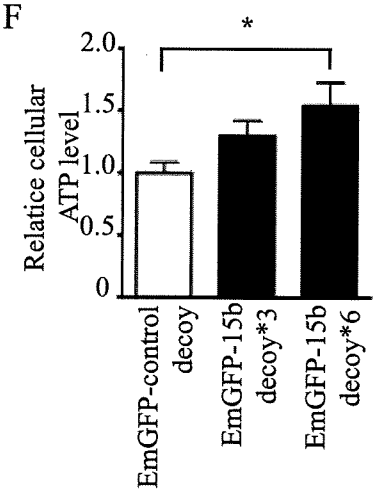

Arl2 siRNA Decreases Cellular ATP Levels without Affecting Cell Viability—Next, the effect of Arl2 siRNA on cellular ATP levels of cardiac myocytes was examined. Cellular ATP levels were reduced by Arl2 siRNA compared with scrambled siRNA (Fig. 4, *A* and *B*). Because it is known that Arl2 forms a complex with BART, an Arl2-specific effector, and localizes with ANT1 (13), BART was suppressed by siRNA in NRVMs, and the cellular ATP levels were measured. siRNAs against BART clearly suppressed cellular ATP levels (Fig. 4, *C* and *D*). To test whether Arl2 siRNA or BART siRNA affected cell viability, the proportions of viable and dead cells were evaluated using calcein AM and ethidium homodimer dyes, respectively, and lactate dehydrogenase levels in the culture medium were measured. When Arl2 siRNA, BART siRNA, or scrambled siRNA was transduced into NRVMs, there was no difference in the proportions of viable and dead cells or lactate dehydrogenase levels in the medium of Arl2 siRNA, BART siRNA, or scrambled siRNA-transduced cardiomyocytes (Fig. 4, *E* and *F*). These results indicated that Arl2 siRNA and BART siRNA decreased cellular ATP levels without affecting cell viability. Transduction of miR-15b also did not influence cell survival (Fig. 4, *G* and *H*).

To further confirm the specific effect of miR-15b on Arl2, cellular ATP levels were analyzed in cardiomyocytes transduced with miR-15b with or without Arl2. Transduction of Arl2 alone did not change cellular ATP levels (Fig. 4, *I* and *J*). Cellular ATP levels in miR-15b-transduced cardiomyocytes recovered to the same level as in control cardiomyocytes after the transduction of Arl2 (Fig. 4*K*). The same results were also seen for the transduction of Arl2 siRNA with or without Arl2 (Fig. 4*L*). Because Arl2 alone did not increase cellular ATP levels (Fig. 4*J*), the present data indicate that the down-regulation of Arl2 protein is the main upstream mechanism that explains how miR-15b reduces cellular ATP levels without affecting cell viability in NRVMs.

Endogenous miR-15b Modulates Cellular ATP Levels—To assess the functional consequences of silencing endogenous miR-15b and miRNAs with the same seed sequence *in vitro*, cardiac myocytes infected with a lentiviral vector were used in which a 3′-UTR with three or six tandem sequences complementary to miR-15b was linked to the luciferase reporter gene or EmGFP (*Luc/EmGFP-15b decoy*3* or -*6*, Fig. 5*A*). The complementary sequences acted as a decoy and sequestered endogenous miR-15b and miRNAs that had the same seed sequence. When miR-15b, -16, -195, and -424 were transfected into 293FT cells along with Luc-15b decoy*3 or *6, luciferase activity was significantly reduced (Fig. 5*B*). On the other hand, miR-1, -133a, -133b, and -21, which have different seed sequences, did not affect the luciferase activity induced by Luc-15b decoy*3 or *6 (Fig. 5*B*). Next, Luc-15b decoy*3 or *6 was transfected into primary cardiomyocytes and 293FT cells. The reduction of luciferase activity indicated that cardiomyocytes expressed miR-15b or a related miRNA(s), and 15b decoys can react with endogenous miRNAs (Fig. 5*C*). Next, we confirmed that an increased concentration of GFP-15b decoy*6 reduced the effect of miR-15b on the luciferase activity of Arl2–3′-UTR Luc (Fig. 5*D*). The cellular Arl2 protein and cellular ATP levels also increased after the transduction of 15b decoy*6 (Fig. 5, *E* and *F*). The present data indicate that miR-15b, -16, -195, and -424 can modulate cellular ATP levels in the heart by targeting Arl2.

miR-15b and Knockdown of Arl2 Changes Mitochondrial Morphology—Changes in the morphology of mitochondria after transduction of miR-15b and Arl2 siRNA were examined further. When compared with cardiomyocytes that had been transduced with miR-control (Fig. 6*A*) or scrambled siRNA (Fig. 6*C*), cells that expressed miR-15b (Fig. 6*B*) and Arl2 siRNA (Fig. 6*D*) had small mitochondria (Fig. 6*E*) and much more degenerated mitochondria (Fig. 6*F*), whereas the number of mitochondria was not significantly different (Fig. 6*G*). These findings suggest that miR-15b is involved in the maintenance of mitochondrial morphology via Arl2. Moreover, ANT activities, and particularly the exchange of ADP/ATP, were suppressed in mitochondria that had been isolated from NRVMs transduced with miR-15b and Arl2 siRNA (Fig. 6*H*). miR-15b and Arl2 siRNA did not change the expression of ANT1 at mRNA or protein levels (data not shown).

DISCUSSION

A growing body of evidence indicates that metabolic and cellular signals influence mitochondrial dynamics, and this could lead to a new understanding of how changes in mitochondria can have a profound impact on their functional output (23). Previously, reduced size, increased number, and structural alterations of cardiac mitochondria have been described in the failing heart (24). It has also been shown that mitochondrial injury is correlated with indices of ventricular dysfunction, such as ejection fraction and end-diastolic pressure, and with the degree of excess orthosympathetic stimulation in congestive heart failure (25). Moreover, reduced expression levels of mitochondrial proteins implicated in ADP rephosphorylation due to reduced gene transcription have been detected during the transition from left ventricular hypertrophy to failure (26). The mechanisms that regulate mitochondrial morphology, size, and number in heart failure are not completely understood, but evidence to date suggests that the morphology of the machinery is modulated through the use of post-translational modifications (27, 28). Therefore, it was hypothesized that miRNAs may influence mitochondrial morphology or function, especially in

FIGURE 5. **Loss of miR-15b, -16, -195, and -424 function increases both Arl2 gene expression and cellular ATP levels.** *A*, the structure of "15b decoy" is shown. *CMV*, cytomegalovirus. *B*, 293FT cells were transfected with a luciferase decoy construct (Luc-15b decoys or Luc-control decoy) along with an expression plasmid for individual miRNAs or miR-control (*control*). *C*, Luc-15b decoys and Luc-control decoy were transfected into 293FT cells or NRVMs. Data are presented as the mean ± S.E. of three independent experiments (***, $p < 0.001$ *versus* Luc-control decoy). *D*, 293FT cells were co-transfected with Arl2–3′-UTR Luc (0.1 μg) and either miR-15b or miR-control (0.1 μg) along with increasing doses of EmGFP-15b decoy*6 (from 0.05 to 0.1 μg) using FuGENE 6™. The *bar graph* indicates values expressed as relative luciferase activity compared with that with miR-control. Data are presented as the mean ± S.E. of three independent experiments (*, $p < 0.05$; **, $p < 0.01$). NRVMs were transduced with 15b decoys by a lentiviral vector in serum-containing medium. Assays were performed 24 h after transduction. Shown are immunoblots of Arl2 (*E*) and cellular ATP levels of NRVMs (*F*). In *F*, data are presented as the mean ± S.E. of four independent experiments (*, $p < 0.05$).

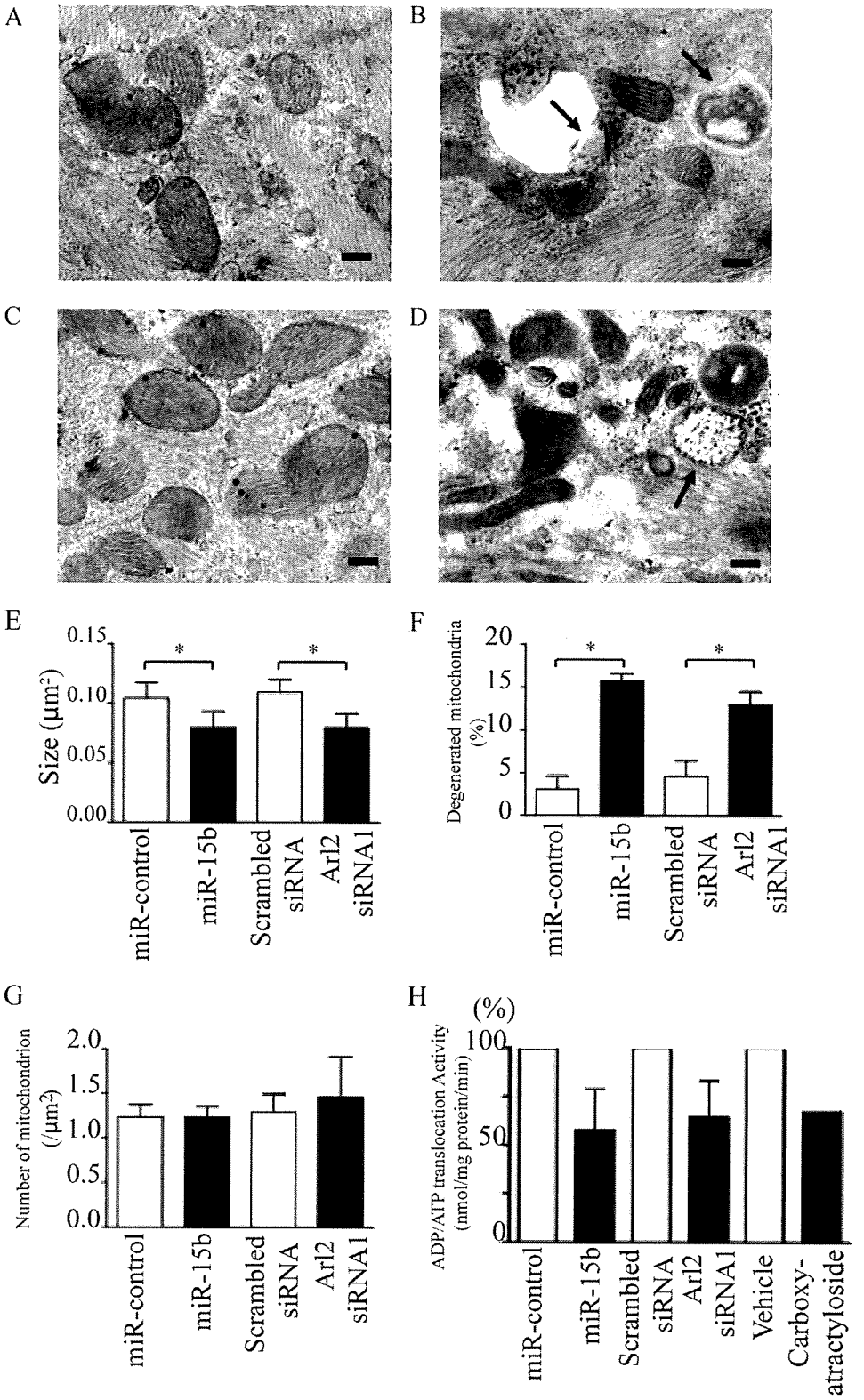

FIGURE 6. **Mitochondria were degenerated by miR-15b or Arl2 siRNA in NRVMs.** Shown are electron microscopy images of NRVMs 72 h after transduction with miR-control (*A*) or miR-15b (*B*) and with scrambled siRNA (*C*) or Arl2 siRNA1 (*D*) using a lentiviral vector. *E–G*, the size (*E*), degenerated proportions (*F*), and number/μm^2 (*G*) of mitochondria in NRVMs are shown. Mitochondria are small, electron-dense, and deformed, and some are completely collapsed or degenerated (*arrows*) in the experimental groups. *Bars* = 200 nm. *, $p < 0.05$. *H*, ANT activities in mitochondria isolated from NRVMs transduced with miR-15b or miR-control and with Arl2 siRNA1 or scrambled siRNA are shown. The values are ADP/ATP exchange activities relative to that of miR-control or scrambled siRNA. Carboxy-atractyloside (0.5 μM) was added 1 min before the addition of external ADP.

failing hearts. The present study focused on the relationship between miRNAs and mitochondria.

In the present study miRNAs were transduced into NRVMs by a lentiviral vector. The transduction efficiency was always >90%, and the lentiviral vectors could express miRNAs at abundant levels that exceeded those of endogenous miRNAs (supplemental Fig. S1). This result implied that these lentiviral vectors could express each miRNA beyond the maximal levels that suppressed target gene expression to minimal levels. Therefore, the expression of each target gene could be suppressed equivalently even if the absolute expression levels of overexpressed miRNAs were different. Several groups have reported that in mice treated with transverse aortic coarctation, an after-loaded cardiac hypertrophy model, miR-15a, -15b, -195, and -424 were up-regulated (1–3). miR-16 is relatively highly expressed in NRVMs (29). Recently, it was reported that miR-195 transgenic mice showed cardiac dysfunction, and the severity depended on the miR-195 expression level (1). Seed sequences of miRNAs, arranged between the second and eighth nucleotides, are the most critical determinant of miRNA targeting as well as evolutionary conservation (12). miR-15a, -15b, -16, -195, -424, and -497 possess the same seed sequence, which implies that these miRNAs have the same target genes, and they are expected to strongly influence their target genes if these miRNAs are regulated in the same manner. These findings suggest that miR-15b, -16, 195, and -424 play important roles in maintaining cardiac integrity. The present results showed that miRNAs, such as miR-15b, -16, -195, and -424, could decrease cellular ATP levels in NRVMs. Although a decoy construct acts by binding and sequestering a specific miRNA, which is fully complementary to the sequence in the decoy, miR-16, -195, and -424, which have the same seed sequence as miR-15b, could

bind 15b decoys. This result was the same as that in a previous report (30), which suggests that the seed sequence plays a critical role in recognition of the target sequence. Therefore, these miRNAs could be blocked by 15b decoys, which could result in an increase in cellular ATP levels. These results suggest that endogenous miR-15b, -16, -195, and -424 modulate cellular ATP levels in NRVMs. In human hematopoietic cancer cells, it has been reported that miR-15 and miR-16 down-regulate Bcl-2 expression post-transcriptionally (21). However, in the present study, miR-15 and miR-16 did not down-regulate Bcl-2 in NRVMs. This discrepancy may be due to the difference between species, tissues, or assay time points. Furthermore, Bcl-2 siRNA did not decrease cellular ATP levels in the present study.

In the present study, we searched for potential target genes by using a combination of three different bioinformatics tools: Target Scan™, PicTar™, and MicroCosm™. miRNAs are fundamentally preserved beyond species, and if the binding site of a miRNA is conserved, the miRNA may regulate target genes in other species. However, miRNA targeting is not based only on conservation of the binding sequence, and the predicted genes are not always the actual targets. Therefore, experimental validations are always required. In this study we found that miR-15b can target Arl2, which is ubiquitously expressed in rodent and human tissues and shows 95% amino acid sequence identity between human and rat (13). Arl2 is a 21-kDa GTPase that associates with a β-tubulin-specific chaperone protein known as cofactor D (31). Moreover, Arl2 forms a complex with BART, an Arl2-specific effector, and localizes with ANT1 (13). Two different isoforms of ANT (ANT1 and ANT2) have been identified in rodents, whereas four isoforms (ANT1–4) are known in humans (32–34). In rodents, ANT1 is the major isoform present in skeletal and cardiac muscle and is also abundant in brain (13, 15, 34, 35). In contrast, murine ANT2 is more widespread than ANT1 but is less prevalent in the heart and skeletal muscle (13, 15, 34, 35). The predominant binding partner for the BART·Arl2 complex is ANT1, whereas the structurally homologous ANT2 protein does not bind to this complex (13).

We found that miR-15b, -16, -195, and -424 have an identical function in the regulation of Arl2. Moreover, a mixture of these miRNAs could decrease mRNA and protein levels of Arl2 and cellular ATP levels in NRVMs as equally as miR-15b, which suggests that these miRNAs did not interfere with each other in Arl2 gene suppression or in the reduction of cellular ATP. The present results also showed that down-regulation of Arl2 or BART leads to cellular ATP reduction in NRVMs. ATP is generated mostly by oxidative phosphorylation via the mitochondrial respiratory chain. ANT exchanges matrix ATP for cytosolic ADP across the inner mitochondrial membrane and plays a central role in oxidative phosphorylation (15). The inhibition of ADP/ATP exchange should deprive ATP synthase of substrate, resulting in a depletion of cellular ATP (36, 37). ANT1 is the predominant mitochondrial inner-membrane protein that is capable of ADP/ATP exchange (15). Cardiac and skeletal muscle mitochondria from ANT1-deficient mice have been shown to have increased levels of Arl2 relative to that seen in mitochondria from wild-type animals (13). The amount of Arl2 in mitochondria is subject to regulation via an ANT1-sensitive pathway in muscle tissues (13). These findings suggest that the interaction between Arl2 and ANT1 could regulate cellular ATP levels.

ANT1-deficient mice and human diseases such as chronic progressive external ophthalmoplegia and Senger syndrome, which can impair the function and expression of ANT1, respectively, are accompanied by hypertrophic cardiomyopathy and various mitochondrial abnormalities in function or morphology (15, 20, 36, 38). This suggests that the dysregulation of ANT1 could cause cardiac hypertrophy associated with impaired mitochondrial integrity. In the present study, miR-15b and Arl2 siRNA caused mitochondrial degeneration and a decrease in ANT activity in NRVMs without affecting ANT1 expression. These findings imply that miR-15b and Arl2 siRNA could decrease cellular ATP levels via ANT1. However, it is still unknown whether the function of Arl2 in ATP production is only due to ANT activity by direct binding because NRVMs transduced with miR-15b and Arl2 siRNA did not enhance the rate of glucose uptake, which would be expected to be accelerated if ATP production is compromised at the level of adenine nucleotide exchange across the mitochondrial membrane (data not shown).

In conclusion, miR-15b, -16, -195, and -424 modulate cellular ATP levels in neonatal rat cardiac myocytes by targeting Arl2. Up-regulation of these miRNAs affects mitochondrial integrity, which may contribute to cardiac dysfunction. A further examination of Arl2 and ANT1 function may lead to a new understanding and therapeutic options for heart diseases.

Acknowledgments—We thank Naoya Sowa and Akemi Fukumoto for excellent technical assistance and Akiko Tsujimoto at Gifu University for the electron microscopy analysis.

REFERENCES

1. van Rooij, E., Sutherland, L. B., Liu, N., Williams, A. H., McAnally, J., Gerard, R. D., Richardson, J. A., and Olson, E. N. (2006) *Proc. Natl. Acad. Sci. U.S.A.* **103,** 18255–18260
2. Sayed, D., Hong, C., Chen, I. Y., Lypowy, J., and Abdellatif, M. (2007) *Circ. Res.* **100,** 416–424
3. Cheng, Y., Ji, R., Yue, J., Yang, J., Liu, X., Chen, H., Dean, D. B., and Zhang, C. (2007) *Am. J. Pathol.* **170,** 1831–1840
4. Sordahl, L. A., McCollum, W. B., Wood, W. G., and Schwartz, A. (1973) *Am. J. Physiol.* **224,** 497–502
5. Heyliger, C. E., Ganguly, P. K., and Dhalla, N. S. (1985) *Can. J. Cardiol.* **1,** 401–408
6. Mercadier, J. J., Lompré, A. M., Wisnewsky, C., Samuel, J. L., Bercovici, J., Swynghedauw, B., and Schwartz, K. (1981) *Circ. Res.* **49,** 525–532
7. Rupp, H., Elimban, V., and Dhalla, N. S. (1992) *FASEB J.* **6,** 2349–2353
8. Scheuer, J., Malhotra, A., Hirsch, C., Capasso, J., and Schaible, T. F. (1982) *J. Clin. Invest.* **70,** 1300–1305
9. Barth, E., Stämmler, G., Speiser, B., and Schaper, J. (1992) *J. Mol. Cell. Cardiol.* **24,** 669–681
10. Johnson, D. T., Harris, R. A., French, S., Blair, P. V., You, J., Bemis, K. G., Wang, M., and Balaban, R. S. (2007) *Am. J. Physiol. Cell Physiol.* **292,** C689–C697
11. Schulz, T. J., Zarse, K., Voigt, A., Urban, N., Birringer, M., and Ristow, M. (2007) *Cell Metab.* **6,** 280–293
12. van Rooij, E., Sutherland, L. B., Qi, X., Richardson, J. A., Hill, J., and Olson, E. N. (2007) *Science* **316,** 575–579
13. Sharer, J. D., Shern, J. F., Van Valkenburgh, H., Wallace, D. C., and Kahn,

R. A. (2002) *Mol. Biol. Cell* **13,** 71–83
14. Chen, X., Van Valkenburgh, C., Fang, H., and Green, N. (1999) *J. Biol. Chem.* **274,** 37750–37754
15. Graham, B. H., Waymire, K. G., Cottrell, B., Trounce, I. A., MacGregor, G. R., and Wallace, D. C. (1997) *Nat. Genet.* **16,** 226–234
16. Hasegawa, K., Meyers, M. B., and Kitsis, R. N. (1997) *J. Biol. Chem.* **272,** 20049–20054
17. Nakagawa, M., Takemura, G., Kanamori, H., Goto, K., Maruyama, R., Tsujimoto, A., Ohno, T., Okada, H., Ogino, A., Esaki, M., Miyata, S., Li, L., Ushikoshi, H., Aoyama, T., Kawasaki, M., Nagashima, K., Fujiwara, T., Minatoguchi, S., and Fujiwara, H. (2008) *Circ. Res.* **103,** 98–106
18. Yanazume, T., Hasegawa, K., Morimoto, T., Kawamura, T., Wada, H., Matsumori, A., Kawase, Y., Hirai, M., and Kita, T. (2003) *Mol. Cell. Biol.* **23,** 3593–3606
19. Passarella, S., Ostuni, A., Atlante, A., and Quagliariello, E. (1988) *Biochem. Biophys. Res. Commun.* **156,** 978–986
20. Dörner, A., and Schultheiss, H. P. (2007) *Trends Cardiovasc. Med.* **17,** 284–290
21. Cimmino, A., Calin, G. A., Fabbri, M., Iorio, M. V., Ferracin, M., Shimizu, M., Wojcik, S. E., Aqeilan, R. I., Zupo, S., Dono, M., Rassenti, L., Alder, H., Volinia, S., Liu, C. G., Kipps, T. J., Negrini, M., and Croce, C. M. (2005) *Proc. Natl. Acad. Sci. U.S.A.* **102,** 13944–13949
22. Das, A. M., and Harris, D. A. (1990) *Biochem. J.* **266,** 355–361
23. Soubannier, V., and McBride, H. M. (2009) *Biochim. Biophys. Acta* **1793,** 154–170
24. Schaper, J., Froede, R., Hein, S., Buck, A., Hashizume, H., Speiser, B., Friedl, A., and Bleese, N. (1991) *Circulation* **83,** 504–514
25. Sabbah, H. N., Sharov, V., Riddle, J. M., Kono, T., Lesch, M., and Goldstein, S. (1992) *J. Mol. Cell. Cardiol.* **24,** 1333–1347
26. Ning, X. H., Zhang, J., Liu, J., Ye, Y., Chen, S. H., From, A. H., Bache, R. J., and Portman, M. A. (2000) *J. Am. Coll. Cardiol.* **36,** 282–287
27. Taguchi, N., Ishihara, N., Jofuku, A., Oka, T., and Mihara, K. (2007) *J. Biol. Chem.* **282,** 11521–11529
28. Zunino, R., Schauss, A., Rippstein, P., Andrade-Navarro, M., and McBride, H. M. (2007) *J. Cell Sci.* **120,** 1178–1188
29. Duisters, R. F., Tijsen, A. J., Schroen, B., Leenders, J. J., Lentink, V., van der Made, I., Herias, V., van Leeuwen, R. E., Schellings, M. W., Barenbrug, P., Maessen, J. G., Heymans, S., Pinto, Y. M., and Creemers, E. E. (2009) *Circ. Res.* **104,** 170–178, 6p following 178
30. Ebert, M. S., Neilson, J. R., and Sharp, P. A. (2007) *Nat. Methods* **4,** 721–726
31. Bhamidipati, A., Lewis, S. A., and Cowan, N. J. (2000) *J. Cell Biol.* **149,** 1087–1096
32. Dörner, A., Olesch, M., Giessen, S., Pauschinger, M., and Schultheiss, H. P. (1999) *Biochim. Biophys. Acta* **1417,** 16–24
33. Dolce, V., Scarcia, P., Iacopetta, D., and Palmieri, F. (2005) *FEBS Lett.* **579,** 633–637
34. Levy, S. E., Chen, Y. S., Graham, B. H., and Wallace, D. C. (2000) *Gene* **254,** 57–66
35. Stepien, G., Torroni, A., Chung, A. B., Hodge, J. A., and Wallace, D. C. (1992) *J. Biol. Chem.* **267,** 14592–14597
36. Wallace, D. C. (2001) *Am. J. Med. Genet.* **106,** 71–93
37. Murdock, D. G., Boone, B. E., Esposito, L. A., and Wallace, D. C. (1999) *J. Biol. Chem.* **274,** 14429–14433
38. Jordens, E. Z., Palmieri, L., Huizing, M., van den Heuvel, L. P., Sengers, R. C., Dörner, A., Ruitenbeek, W., Trijbels, F. J., Valsson, J., Sigfusson, G., Palmieri, F., and Smeitink, J. A. (2002) *Ann. Neurol.* **52,** 95–99

nature neuroscience

Nardilysin regulates axonal maturation and myelination in the central and peripheral nervous system

Mikiko Ohno[1], Yoshinori Hiraoka[1], Tatsuhiko Matsuoka[1], Hidekazu Tomimoto[2], Keizo Takao[3–5], Tsuyoshi Miyakawa[3–5], Naoko Oshima[6], Hiroshi Kiyonari[6], Takeshi Kimura[1], Toru Kita[1,7] & Eiichiro Nishi[1]

Axonal maturation and myelination are essential processes for establishing an efficient neuronal signaling network. We found that nardilysin (N-arginine dibasic convertase, also known as Nrd1 and NRDc), a metalloendopeptidase enhancer of protein ectodomain shedding, is a critical regulator of these processes. *Nrd1*$^{-/-}$ mice had smaller brains and a thin cerebral cortex, in which there were less myelinated fibers with thinner myelin sheaths and smaller axon diameters. We also found hypomyelination in the peripheral nervous system (PNS) of *Nrd1*$^{-/-}$ mice. Neuron-specific overexpression of NRDc induced hypermyelination, indicating that the level of neuronal NRDc regulates myelin thickness. Consistent with these findings, *Nrd1*$^{-/-}$ mice had impaired motor activities and cognitive deficits. Furthermore, NRDc enhanced ectodomain shedding of neuregulin1 (NRG1), which is a master regulator of myelination in the PNS. On the basis of these data, we propose that NRDc regulates axonal maturation and myelination in the CNS and PNS, in part, through the modulation of NRG1 shedding.

Myelination of axons by glial cells, such as oligodendrocytes in the CNS and Schwann cells in the PNS, is essential for rapid impulse conduction. Myelination is coordinated by the interaction between axons and glial cells. Although the diameter of an axon dictates whether myelination is initiated, myelination may further induce radial growth of axons[1,2]. Because axonal conduction is determined by axon caliber and myelin sheath thickness, axonal maturation (radial growth of axon) and myelination are essential processes for establishing an efficient neuronal signaling network[3,4]. Several lines of evidence suggest that bidirectional signaling between axons and myelin maintains neuronal functions. For example, some oligodendrocyte-specific proteins, such as proteolipid protein and 2′,3′-cyclic nucleotide phosphodiesterase (CNP), are required to maintain axonal integrity[5,6]. On the other hand, NRG1, a member of the epidermal growth factor (EGF) family, induces axonal signaling and is required for glial differentiation, proliferation and myelination[7–9]. NRG1 is synthesized as a transmembrane protein and then shed from the cell surface by proteolytic cleavage in the juxtamembrane region[10]. ADAM proteases and BACE1 (β-secretase) have been proposed as sheddases for NRG1 (refs. 11–15). Because BACE1-deficient mice have a hypomyelination phenotype[13–15], shedding of NRG1 is thought to be important in myelination *in vivo*. However, the underlying mechanism by which NRG1 shedding is regulated is poorly understood.

NRDc is a zinc peptidase of the M16 family that selectively cleaves dibasic sites[16,17]. We identified NRDc as a specific binding partner of heparin-binding EGF-like growth factor (HB-EGF) and found that NRDc enhances HB-EGF shedding through activation of tumor necrosis factor α converting enzyme (TACE, also known as ADAM17)[18,19]. We also found that NRDc enhances the ectodomain shedding of multiple membrane proteins, including amyloid precursor protein (APP) and tumor necrosis factor-α, through activation of several ADAM proteases[20,21]. These results suggest that NRDc may regulate the ectodomain shedding of a wide range of membrane proteins. To explore the physiological functions of NRDc, we generated *Nrd1*$^{-/-}$ mice and found that these mice had impaired axonal maturation and hypomyelination in both the CNS and PNS. Furthermore, we found that NRDc regulates axonal maturation and myelination in the CNS and PNS, in part, through the modulation of NRG1 shedding.

RESULTS

Small brains in *Nrd1*$^{-/-}$ mice

NRDc was highly expressed in brain lysates of early postnatal mice but was expressed at a lower level in the brains of adult mice (**Fig. 1a**). Using immunohistochemical analysis, we found that NRDc was expressed in neurons and dendrites but not in glial cells (**Fig. 1b**)[20]. These findings were supported by *in situ* hybridization, which revealed that there was little or no *Nrd1* mRNA in the corpus callosum (**Supplementary Fig. 1**).

To examine the physiological functions of NRDc, we generated *Nrd1*$^{-/-}$ mice by gene targeting (**Supplementary Fig. 2**). No *Nrd1* mRNA or protein was detected by real-time PCR (data not shown) and western blot analysis, respectively, in the brains (**Fig. 1a**) and all other

[1]Department of Cardiovascular Medicine, Graduate School of Medicine, Kyoto University, Sakyo-ku, Kyoto, Japan. [2]Department of Neurology, Graduate School of Medicine, Mie University, Tsu, Japan. [3]Division of Systems Medical Science, Institute for Comprehensive Medical Science, Fujita Health University, Toyoake, Aichi, Japan. [4]Japan Science and Technology Agency (JST), Institute for Bioinformatics Research and Development and Core Research for Evolutional Science and Technology, Kawaguchi, Saitama, Japan. [5]Frontier Technology Center, Graduate School of Medicine, Kyoto University, Sakyo-ku, Kyoto, Japan. [6]Laboratory for Animal Resources and Genetic Engineering, Center for Developmental Biology, RIKEN Kobe, Chuo-ku, Kobe, Japan. [7]Present address: Kobe City Medical Center General Hospital, Chuo-ku, Kobe, Japan. Correspondence should be addressed to E.N. (nishi@kuhp.kyoto-u.ac.jp).

Received 29 July; accepted 22 September; published online 22 November 2009; doi:10.1038/nn.2438

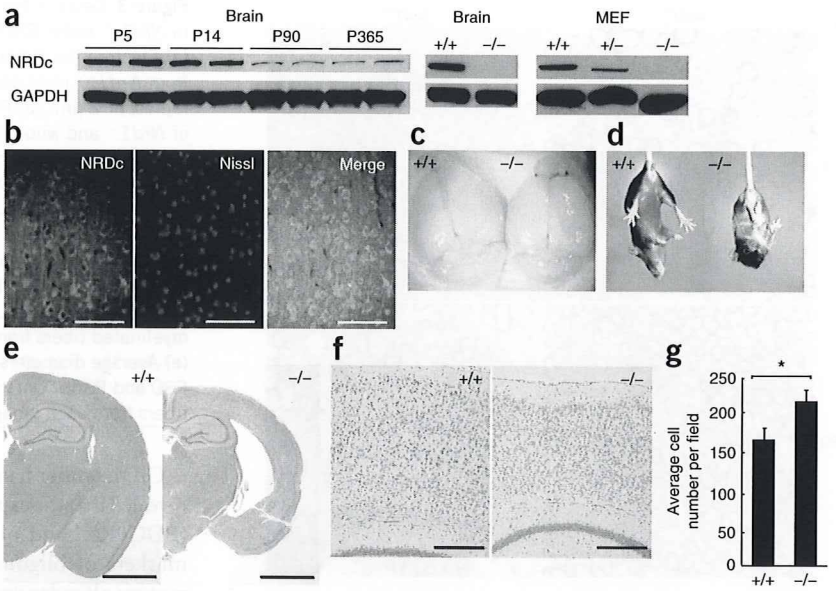

Figure 1 Expression of NRDc in brains and gross CNS phenotypes of *Nrd1*$^{-/-}$ mice. (**a**) Immunoblot analysis of brain extracts (left, center) or total cell extracts (right) stained with antibodies to NRDc and GAPDH. Analysis of brain extracts from wild-type mice at P5, P14, P90 and P365 (left) and from control wild-type (+/+) and *Nrd1*$^{-/-}$ mice (−/−) at P90 (center). Analysis of the total extracts of MEFs isolated from *Nrd1*$^{+/+}$, *Nrd1*$^{+/-}$ or *Nrd1*$^{-/-}$ mice (right). Full-length blots are presented in **Supplementary Figure 9**. (**b**) Immunohistochemistry using an antibody to NRDc (green) with cerebral cortex sections from wild-type mice at P30. The section was double-stained with fluorescent Nissl (red). Scale bars represent 250 μm. (**c**) Brains of *Nrd1*$^{-/-}$ mice and control wild-type littermates at P90. (**d**) Enhanced limb-clasping reflex of *Nrd1*$^{-/-}$ compared with wild-type mice at P42. (**e**) Hematoxylin and eosin–stained sections of one brain hemisphere of *Nrd1*$^{-/-}$ mice and wild-type littermates at P90. An enlargement of the lateral ventricles and cortical shrinkage in *Nrd1*$^{-/-}$ brain is shown. Scale bars represent 2 mm. (**f**,**g**) Nissl-stained sections of cerebral cortex of *Nrd1*$^{-/-}$ mice and wild-type littermates at P90. Scale bars represent 500 μm. Counting of Nissl-positive neurons at the same bregma levels (six non-overlapping fields, $n = 2$ per genotype, results are mean ± s.e.m., * $P < 0.01$) revealed that there was a greater neuronal cell density in the *Nrd1*$^{-/-}$ cortex.

tissues tested from *Nrd1*$^{-/-}$ mice (data not shown). Immunostaining of tissue sections also showed a lack of NRDc protein in the cerebral cortex of *Nrd1*$^{-/-}$ mice (**Supplementary Fig. 2**). The levels of NRDc protein in embryonic fibroblasts (MEFs) isolated from *Nrd1*$^{+/+}$, *Nrd1*$^{+/-}$ or *Nrd1*$^{-/-}$ mice correlated with the predicted gene dosage of *Nrd1* in these mice (**Fig. 1a**).

Pups lacking NRDc were born at the expected Mendelian ratio. However, approximately 80% died within 48 h of birth. *Nrd1*$^{-/-}$ pups weighed approximately 30% less than *Nrd1*$^{+/+}$ and *Nrd1*$^{+/-}$ littermates, indicating that NRDc is indispensable for normal prenatal growth. The *Nrd1*$^{-/-}$ mice that survived remained smaller than their wild-type and heterozygous littermates throughout postnatal development and had average brain weights that were 29% lower than those of *Nrd1*$^{+/+}$ mice at postnatal day 90 (P90) (*Nrd1*$^{+/+}$, 521.0 ± 30.0 mg; *Nrd1*$^{-/-}$, 371.5 ± 16.8 mg; $n = 5$, $P < 0.001$; **Fig. 1c**). Although the *Nrd1*$^{-/-}$ mice that survived lived until 2 years of age, they had several prominent neurological disorders. For example, *Nrd1*$^{-/-}$ mice exhibited enhanced limb-clasping reflexes when suspended by the tail, whereas control mice extended their limbs (**Fig. 1d**).

To assess the underlying neuropathology, we examined the brains of *Nrd1*$^{-/-}$ mice histologically. Although the gross anatomy of the *Nrd1*$^{-/-}$ mouse brain was normal at P1, P14 and P30 (**Supplementary Fig. 3**), we observed a thin cerebral cortex and enlarged lateral ventricles at P90 (**Fig. 1e**). We found that the *Nrd1*$^{-/-}$ cortex had a greater neuronal cell density than in the *Nrd1*$^{+/+}$ cortex by Nissl staining (**Fig. 1f,g**). Furthermore, there were no differences in the number of TUNEL-positive cells detected in the cortex of *Nrd1*$^{+/+}$ and *Nrd1*$^{-/-}$ mice (data not shown), indicating that there was no excessive loss of neurons in the *Nrd1*$^{-/-}$ cortex.

Hypomyelination in the CNS of *Nrd1*$^{-/-}$ mice

We next examined the integrity of axons and myelin using silver impregnation and luxol fast blue (LFB) staining, respectively. We detected much less silver impregnation in *Nrd1*$^{-/-}$ brains, especially in the corpus callosum and cortical layers adjacent to it

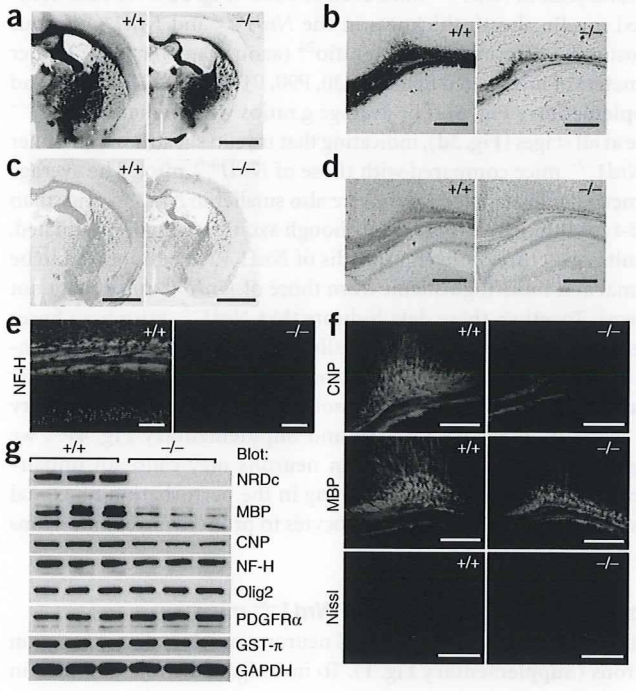

Figure 2 Impaired axonal maturation and hypomyelination in the CNS of *Nrd1*$^{-/-}$ mice. (**a**–**d**) Silver impregnation by Bielschowskey method (**a**,**b**) and LFB staining (**c**,**d**) of *Nrd1*$^{-/-}$ brain (−/−) and wild-type brain (+/+) at P90. We found impairment of axonal maturation and hypomyelination in *Nrd1*$^{-/-}$ brains, especially in the corpus callosum. (**e**,**f**) Immunohistochemistry using antibodies to NF-H (**e**), CNP and MBP (**f**) of corpus callosum from control wild-type mice and *Nrd1*$^{-/-}$ mice at P30. Scale bars represent 2 mm (**a**,**c**), 500 μm (**b**,**d**,**f**) and 250 μm (**e**). (**g**) Immunoblot analysis of brain extracts from wild-type and *Nrd1*$^{-/-}$ brains at P14 showed a reduction of MBP, CNP and NF-H expression in *Nrd1*$^{-/-}$ brains. On the other hand, there were no differences in Olig2, PDGFRα and GST-π expression ($n = 3$ in each genotype). Full-length blots are presented in **Supplementary Figure 9**.

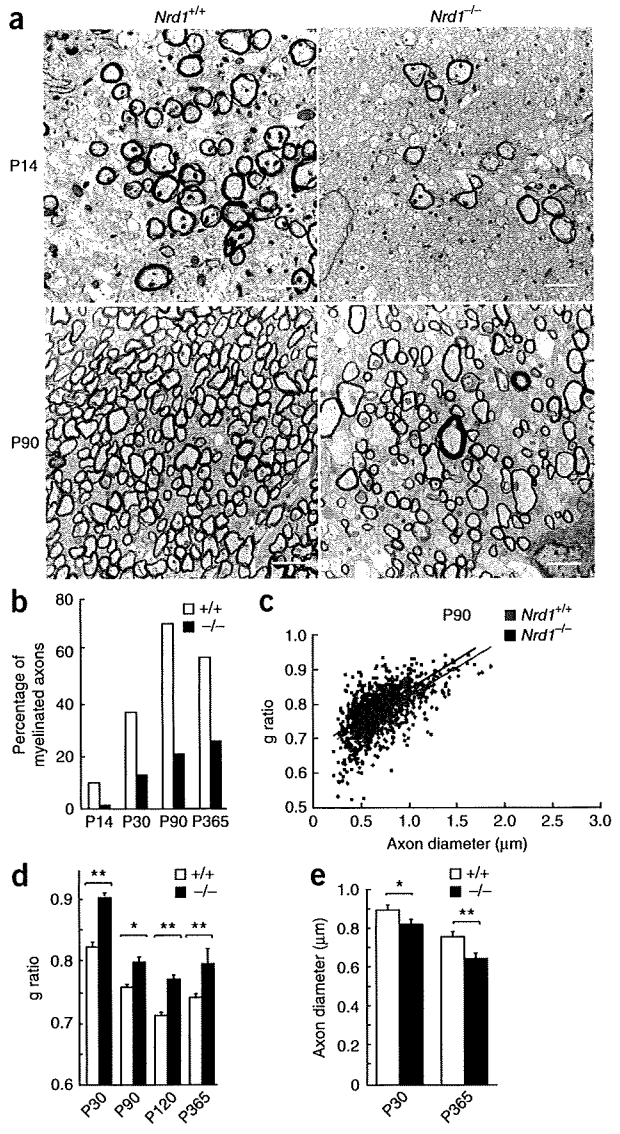

Figure 3 Delay in the initiation of myelination and hypomyelination in *Nrd1*$^{-/-}$ mice. Electron microscopic analysis of corpus callosum. (**a**) Electron micrographs of transverse sections at the corpus callosum from *Nrd1*$^{-/-}$ mice and wild-type littermates at P14 and P90. Scale bars represent 2 μm. (**b**) Percentage of myelinated axons in the corpus callosum of *Nrd1*$^{-/-}$and wild-type littermates at P14, P30, P90 and P365. (**c**,**d**) Quantitation of myelin sheath thickness in the corpus callosum by analyzing g ratios with electron micrographs. Scatter plots of myelin thickness, expressed as g ratios, against axon diameters at P90 in *Nrd1*$^{-/-}$ (black) and wild-type (red) corpus callosum are shown (**c**). We determined the average myelin sheath thickness (g ratio) of myelinated fibers at P30, P90, P120 and P365 and found hypomyelination in the corpus callosum of *Nrd1*$^{-/-}$ mice (**d**). Data represent the mean ± s.e.m. for 300–900 myelinated fibers from each group. * $P < 0.03$ and ** $P < 0.0001$. (**e**) Average diameters of myelinated axons in the corpus callosum at P30 and P365. Data represent the mean ± s.e.m. for 300–900 myelinated fibers from each group. * $P = 0.0002$ and ** $P < 0.0001$.

(**Fig. 2a**,**b**). Similarly, LFB staining was markedly weaker in this region (**Fig. 2c**,**d**). These results suggest that the volume of axons and myelin in *Nrd1*$^{-/-}$ brain is decreased, especially in the corpus callosum. Furthermore, expression of the axonal marker neurofilament-H (NF-H; **Fig. 2e**) and the myelin markers CNP and myelin basic protein (MBP) (**Fig. 2f**) were lower in the corpus callosum in *Nrd1*$^{-/-}$ brain at P30. Using western blotting, we found reduced CNP and MBP protein levels at an earlier stage (P14) in *Nrd1*$^{-/-}$ brain extracts (**Fig. 2g**), suggesting that *Nrd1*$^{-/-}$ mice have a severe impairment of axonal maturation and hypomyelination starting at the early stages of these processes. Neuronal expression of NRDc was detected in whole regions of the brain, but there were some prominent regional differences. For example, NRDc was highly expressed in cortical neurons, but neurons in striatum expressed relatively low levels of NRDc (**Supplementary Fig. 4**), similar to the expression pattern seen in human brain[22]. Consistent with these results, the myelination defect in *Nrd1*$^{-/-}$ striatum was not as obvious as the defect in the cortex, hippocampus and corpus callosum (**Supplementary Fig. 4**). These results suggest that there is a correlation between the expression level of NRDc and the extent of the myelination defect in *Nrd1*$^{-/-}$ mice.

On the other hand, western blots of the same set of brain extracts revealed that the expression of platelet-derived growth factor receptor α (PDGFRα) and oligodendrocyte transcription factor 2 (Olig2)[23], markers of oligodendrocyte precursors, and GST-π, a marker of mature oligodendrocyte, were not reduced in *Nrd1*$^{-/-}$ mice (**Fig. 2g**), suggesting that oligodendroglial differentiation is normal in *Nrd1*$^{-/-}$ mice. Moreover, we found via quantitative analysis of Olig2-positive cells at embryonic day 18.5 (E18.5) and P5 that there were no differences in the number of oligodendrocyte precursors in *Nrd1*$^{+/+}$ and *Nrd1*$^{-/-}$ brains (**Supplementary Fig. 5**). These data suggest that NRDc affects myelination, but not differentiation of oligodendrocytes.

To obtain direct evidence of impaired axonal maturation and hypomyelination in the CNS, we analyzed sections of the corpus callosum in *Nrd1*$^{-/-}$ mice and *Nrd1*$^{+/+}$ littermates between P14 and P365 by electron microscopy (**Fig. 3a** and **Supplementary Fig. 6**). The proportion of myelinated axons was markedly reduced in *Nrd1*$^{-/-}$ mice at all of the stages examined (**Fig. 3b**). At P14, only about one seventh of the *Nrd1*$^{-/-}$ axons were myelinated compared with the *Nrd1*$^{+/+}$ axons, indicating that there was a substantial delay in the initiation of myelination in *Nrd1*$^{-/-}$ mice. The proportion of myelinated axons in the *Nrd1*$^{-/-}$ CNS was only 21.0% at P90 and did not approach the level seen in *Nrd1*$^{+/+}$ mice even at P365 (**Fig. 3b**). We next compared myelin sheath thickness in the *Nrd1*$^{-/-}$ and *Nrd1*$^{+/+}$ corpus callosum by determining the g ratio[24] (axon diameter to total fiber diameter) of myelinated fibers at P30, P90, P120 and P365 (**Fig. 3c** and **Supplementary Fig. 6**). The average g ratios were higher in *Nrd1*$^{-/-}$ mice at all stages (**Fig. 3d**), indicating that myelin sheaths were thinner in *Nrd1*$^{-/-}$ mice compared with those of *Nrd1*$^{+/+}$ mice. The average diameters of myelinated axons were also smaller in *Nrd1*$^{-/-}$ mice than wild-type littermates (**Fig. 3e**). Although axons were hypomyelinated, the ultrastructure of myelin sheaths of *Nrd1*$^{-/-}$ mice appeared to be normal and indistinguishable from those of *Nrd1*$^{+/+}$ mice (data not shown). Together, these data indicate that *Nrd1*$^{-/-}$ mice have fewer myelinated fibers in the corpus callosum, and the fibers have thinner myelin sheaths and smaller axon diameters. As NRDc is highly expressed in neurons, but either not expressed or expressed at very low levels in glial cells (**Fig. 1b** and **Supplementary Fig. 4**)[20], we propose that the loss of NRDc in neurons may cause an impairment of axonal maturation, resulting in the perturbation of axonal signaling required for oligodendrocytes to properly myelinate axons and hypomyelination.

Hypomyelination in the PNS of *Nrd1*$^{-/-}$ mice

NRDc was also expressed in spinal neurons and dorsal root ganglion neurons (**Supplementary Fig. 1**). To investigate the role of NRDc in

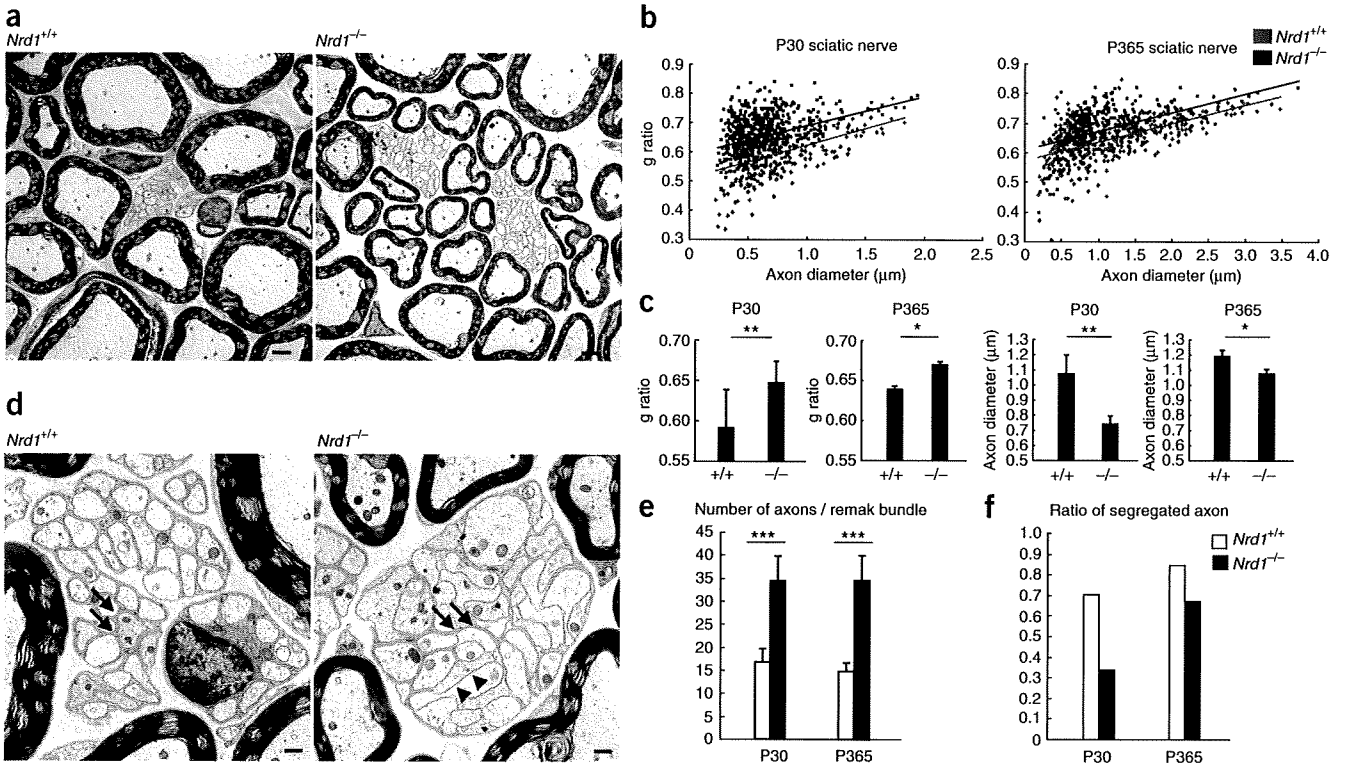

Figure 4 Impaired axonal maturation and hypomyelination in the PNS of *Nrd1*$^{-/-}$ mice. (**a**) Electron micrographs of sciatic nerves of *Nrd1*$^{+/+}$ and *Nrd1*$^{-/-}$ mice at P365 showed obvious hypomyelination in the *Nrd1*$^{-/-}$ nerves. Scale bars represent 2 μm. (**b**) Scatter plots of g ratios and axon diameters at P30 and P365 of *Nrd1*$^{-/-}$ and wild-type sciatic nerves. (**c**) G ratios and axon diameters at P30 and P365 of *Nrd1*$^{+/+}$ and *Nrd1*$^{-/-}$ sciatic nerves. Data represent the mean ± s.e.m. for 750 myelinated fibers from each group ($n = 4$ for each genotype). * $P < 0.03$ and ** $P < 0.01$. (**d**) Electron micrographs of Remak bundles in sciatic nerves showed altered axonal segregation in *Nrd1*$^{-/-}$ bundles. Arrows indicate Schwann cell cytoplasmic processes between different axons. Note that many axons of *Nrd1*$^{-/-}$ bundles are directly apposed without the cytoplasmic processes (arrowhead). Scale bars represent 500 nm. (**e**) The average numbers of axons in a Remak bundle at P30 and P365 were significantly reduced in *Nrd1*$^{-/-}$ sciatic nerves. Data represent the mean ± s.e.m. for 150–300 Remak bundle from each group ($n = 2$ for each genotype). *** $P < 0.0001$. (**f**) Ratios of segregated axons in *Nrd1*$^{-/-}$ sciatic nerves at P30 and P365 were reduced (150–300 Remak bundle from each group, $n = 2$ for each genotype).

axonal maturation and myelination in the PNS, we analyzed the sciatic nerves of *Nrd1*$^{-/-}$ mice by electron microscopy and found that the sciatic nerves of *Nrd1*$^{-/-}$ mice were hypomyelinated (**Fig. 4a**). Quantitative analysis by measuring the g ratio of myelinated fibers indicated that the myelin sheath thickness was thinner in *Nrd1*$^{-/-}$ mice at both P30 and P365. The diameter of myelinated axons was also smaller in *Nrd1*$^{-/-}$ nerves compared with *Nrd1*$^{+/+}$ nerves (**Fig. 4b,c**).

We also examined the morphology of Remak bundles (**Fig. 4d–f**). Remak bundles in *Nrd1*$^{-/-}$ nerves contained approximately two-fold more axons than *Nrd1*$^{+/+}$ nerves at P30 and P365 (**Fig. 4d,e**). In addition, there were many unsegregated or poorly segregated axons that lacked intervening Schwan cell processes in *Nrd1*$^{-/-}$ bundles (**Fig. 4d,f**). These findings indicate that NRDc is critical for axonal maturation and myelination of both the CNS and PNS. Notably, the observed hypomyelination and morphological changes of Remak bundles in the PNS of *Nrd1*$^{-/-}$ mice were very similar to those described in *Nrg1*$^{+/-}$ and *Bace1*$^{-/-}$ mice[7,8,13,14,25].

The level of neuronal NRDc regulates myelin thickness

To determine the dose-dependent effects of NRDc expression on the CNS phenotypes, we examined brains from *Nrd1*$^{+/-}$ mice, in which NRDc expression was obviously reduced (**Fig. 5a**). The gross anatomy of *Nrd1*$^{+/-}$ brains showed no cortical shrinkage, but we did find enlarged lateral ventricles (**Fig. 5b**). Although we detected no obvious differences between *Nrd1*$^{+/+}$ and *Nrd1*$^{+/-}$ brains by LFB staining (**Fig. 5b,c**), we did find decreased expression of the myelin and axon markers MBP and NF-H in *Nrd1*$^{+/-}$ corpus callosum by immunostaining (**Fig. 5d,e**). These findings were confirmed by western blot using whole brain lysates (**Fig. 5f**). Furthermore, we analyzed *Nrd1*$^{+/-}$ corpus callosum by electron microscopy and found that the myelin sheath thickness of *Nrd1*$^{+/-}$ mice was significantly thinner than that of *Nrd1*$^{+/+}$ mice (average g ratio: *Nrd1*$^{+/+}$, 0.725 ± 0.020 s.e.m.; *Nrd1*$^{+/-}$, 0.761 ± 0.001 s.e.m.; $n > 1000$ fibers from each group, $P < 0.0001$; **Fig. 5g,h**). The axon diameters of *Nrd1*$^{+/-}$ mice were also smaller compared with those of *Nrd1*$^{+/+}$ mice (*Nrd1*$^{+/+}$, 0.650 ± 0.018 μm; *Nrd1*$^{+/-}$, 0.582 ± 0.006 μm; $P < 0.0001$). Thus, *Nrd1*$^{+/-}$ mice have a CNS phenotype that is intermediate of those of *Nrd1*$^{+/+}$ and *Nrd1*$^{-/-}$ mice, indicating that the level of NRDc expression in neurons affects axonal maturation and myelination.

Our loss-of-function approach using *Nrd1*$^{-/-}$ mice revealed that NRDc is essential for axonal maturation and myelination in the CNS. To further define the role of NRDc in these processes, we used a gain-of-function approach with transgenic mice that overexpress mouse NRDc under the control of the *Camk2a* promoter (NRDc-Tg mice)[26,27]. Western blot analysis of whole brain extract of NRDc-Tg mice at P90 revealed that there was an increase in NRDc expression in the transgenic mice (**Fig. 6a**). The *Camk2a* promoter was specifically activated in neurons of cerebral cortex and hippocampus[26,27], where the increased expression of NRDc was confirmed by immunostaining (**Fig. 6b,c**). To see the regional effect of NRDc

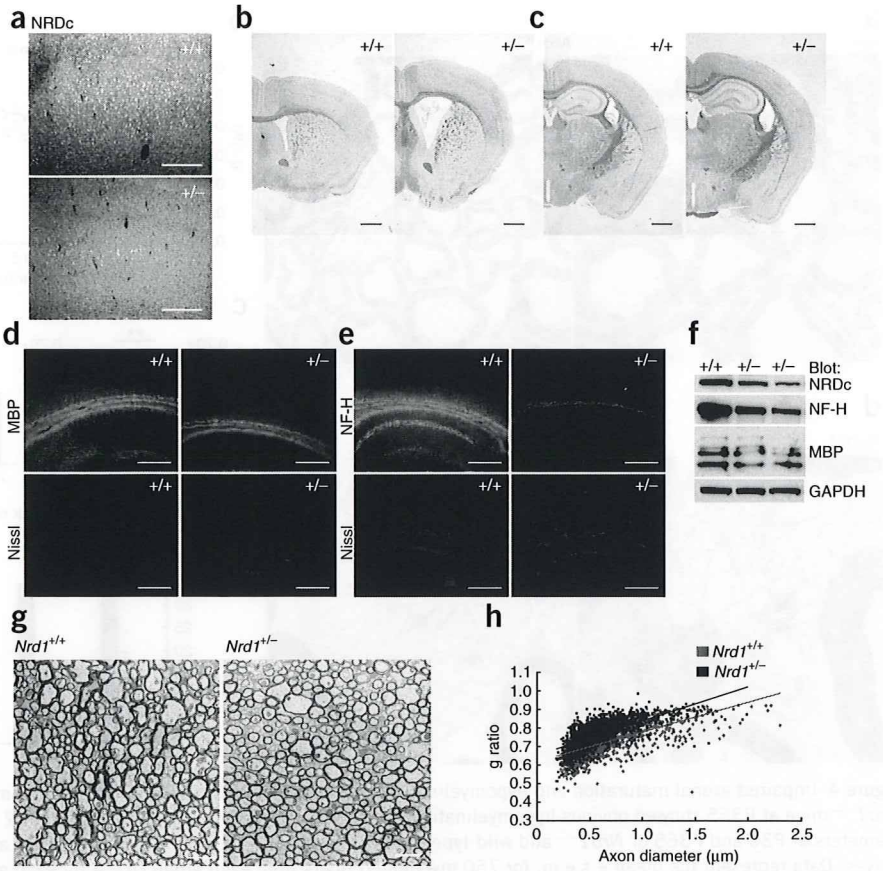

Figure 5 Intermediate CNS phenotype in *Nrd1*$^{+/-}$ mice. (**a**) Immunohistochemistry of *Nrd1*$^{+/-}$ cortex (+/–) with antibody to NRDc showed the obvious reduction of NRDc expression. (**b**,**c**) LFB staining of *Nrd1*$^{+/-}$ brains showed enlarged lateral ventricles, especially in the frontal section (**b**), compared with wild-type brains, but no obvious cortical shrinkage. Scale bars represent 1 mm. (**d**,**e**) Immunohistochemistry of *Nrd1*$^{+/+}$ and *Nrd1*$^{+/-}$ corpus callosum at P90 using antibodies to MBP (**d**) and NF-H (**e**) showed a decrease in the expression of these axonal and myelin markers in *Nrd1*$^{+/-}$ brain. The sections were double-stained with fluorescent Nissl. Scale bars represent 500 μm. (**f**) Immunoblot analysis of whole-brain extracts using antibodies to NRDc, NF-H and MBP. Expression of these proteins was reduced in *Nrd1*$^{+/-}$ brains compared with wild-type littermates. Full-length blots are presented in **Supplementary Figure 9**. (**g**) Electron micrographs of *Nrd1*$^{+/+}$ and *Nrd1*$^{+/-}$ corpus callosum at P120. Scale bars represent 2 μm. (**h**) Scatter plots of g ratio against axon diameters of *Nrd1*$^{+/+}$ and *Nrd1*$^{+/-}$ corpus callosum at P120.

overexpression, we divided mouse brains into two regions: cerebral cortex plus hippocampus (frontal region) and brain stem plus cerebellum (posterior region). Using western blot, we found increased expression of NRDc protein only in the frontal region (**Fig. 6d**). The expression of the myelin markers MBP and CNP was also increased in the frontal region, but not in the posterior region (**Fig. 6d**). We detected higher expression of MBP in corpus callosum by immunostaining (**Fig. 6e**). Notably, analysis of myelination in the NRDc-Tg corpus callosum by electron microscopy revealed that the average g ratio was significantly lower than in wild type, indicating that the myelin sheaths were thicker in NRDc-Tg mice than in wild types (**Fig. 6f–h**). On the other hand, there was no significant difference in the diameter of myelinated axons in the corpus callosum between the NRDc-Tg and wild-type mice (average diameter: wild type, 0.80 ± 0.39 μm; NRDc-Tg, 0.81 ± 0.39 μm, $P = 0.654$). These results provide further evidence that the level of neuronal NRDc regulates myelin sheath thickness. The *Camk2a* promoter is activated around P5, which is after the differentiation of neuronal cells and before subcortical myelination[27]. Thus, NRDc probably affects myelination by regulating axonal signals transmitted from differentiated neurons.

Impaired motor activity and cognitive deficits in *Nrd1*$^{-/-}$ mice

To examine the effect of NRDc on neurological functions, we analyzed *Nrd1*$^{-/-}$ mice with a battery of behavioral tests[28]. We examined neuromuscular strength with grip strength and wire-hanging tests. Although *Nrd1*$^{-/-}$ mice had reduced grip strength (**Fig. 7a**), we found no difference between *Nrd1*$^{+/+}$ and *Nrd1*$^{-/-}$ mice in the wire-hanging test (**Supplementary Fig. 7**), indicating that *Nrd1*$^{-/-}$ mice possess sufficient grip strength to hold their body weight. We next assessed motor coordination and balance with the beam test and rotarod test[29]. In the beam test, *Nrd1*$^{-/-}$ mice moved much slower and slipped more frequently than *Nrd1*$^{+/+}$ mice (**Fig. 7b**,**c**). *Nrd1*$^{-/-}$ mice also had a shorter latency to fall in the rotarod test (**Fig. 7d**). These results indicate that there is a severe impairment of motor coordination and balance in the *Nrd1*$^{-/-}$ mice.

In contrast with motor activity, sensory pathways were apparently conserved in *Nrd1*$^{-/-}$ mice, as their reactions were similar to those of *Nrd1*$^{+/+}$ mice in the hot-plate test (**Supplementary Fig. 7**). We examined cognitive functions of *Nrd1*$^{-/-}$ mice with the T-maze test, in which working memory and reference memory are evaluated by a forced-alternation task and a left right–discrimination task, respectively[30]. In both tasks, *Nrd1*$^{-/-}$ mice took much longer to complete a session, probably as a result of impaired motor activity (**Supplementary Fig. 7** and data not shown). Although the percentage of correct choices in the forced-alternation task was lower in *Nrd1*$^{-/-}$ mice, there were no differences in the left right–discrimination task between *Nrd1*$^{+/+}$ and *Nrd1*$^{-/-}$ mice (**Fig. 7e**,**f**). Together, these results suggest that reference memory is preserved, whereas working memory is impaired in *Nrd1*$^{-/-}$ mice. Although these behavioral alterations are consistent with the axonal and myelination defects, spinal or cerebellar defects might also influence the overall performance of *Nrd1*$^{-/-}$ mice.

NRDc regulates NRG1 shedding through BACE1 and TACE

NRG1, one of the master regulators of myelination, is synthesized as a transmembrane protein and then proteolytically shed from the cell surface[8,10]. Recent reports of hypomyelination in *Bace1*$^{-/-}$ mice have implicated BACE1 in NRG1 shedding[13–15]. NRG1 is also shed from the cell surface by TACE[11], although there is no information about nervous system phenotypes of TACE-deficient mice as a result of their early lethality. These findings, along with the potentiating effect of NRDc on protein ectodomain shedding[19–21], prompted us to examine whether NRDc affects axonal maturation and myelination via regulation of NRG1 shedding by BACE1 or TACE. To determine whether NRDc potentiates BACE1/TACE activity, we carried out transfection experiments in COS7 cells. NRG1 type I was tagged with hemagglutinin (HA) at the

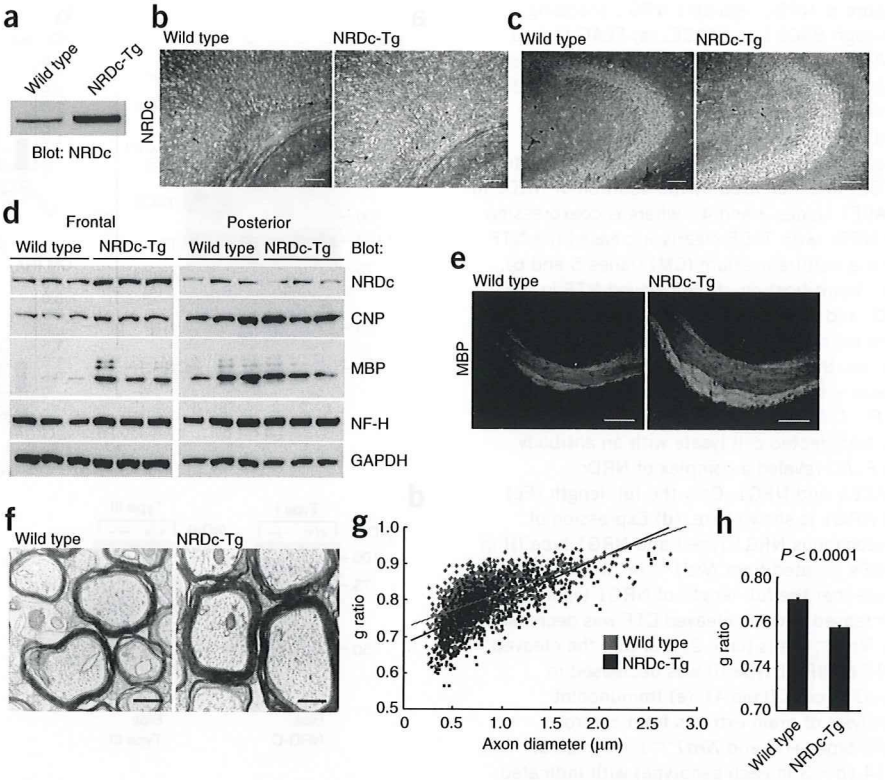

Figure 6 Transgenic overexpression of neuronal NRDc induces hypermyelination in the CNS. (**a**) Immunoblot analysis of total brain extracts from wild-type littermates and NRDc-Tg mice at P90 with antibody to NRDc. (**b**,**c**) We stained sections from NRDc-Tg brains with an antibody to NRDc and found neuronal overexpression of NRDc in the cortex (**b**) and hippocampus (**c**) compared with wild-type brains. Scale bars represent 250 μm. (**d**) Brains of wild-type and NRDc-Tg mice were divided into two regions at the border of cerebral cortex and cerebellum. We analyzed total brain extracts from frontal region and posterior region by immunoblot using antibodies to NRDc, CNP, MBP and NF-H. Note that the increased expression of NRDc, CNP and MBP were only detected in the frontal region. Full-length blots are presented in **Supplementary Figure 9**. (**e**) Expression of MBP in the corpus callosum was increased in NRDc-Tg compared with wild type mice. Scale bars represent 500 μm. (**f**) Electron micrographs of corpus callosum from NRDc-Tg and wild type mice at P30. Scale bars represent 500 nm. (**g**,**h**) Myelin sheaths were thicker in NRDc-Tg mice than in wild types. Scatter plots of g ratios against axon diameters at P30 in NRDc-Tg and wild-type corpus callosum (**g**) and the average g ratio (**h**) are shown. Data represent the mean ± s.e.m. for no fewer than 1,000 myelinated fibers from each group ($n = 4$ for each genotype).

N terminus so that the full length and N-terminal fragment (NTF) of NRG1 type I could be detected with an antibody to HA. Coexpression of NRDc and BACE1 increased NTF levels in total cell lysates, but not in the culture medium (**Fig. 8a**,**b**). In contrast, coexpression of NRDc with TACE clearly increased NTF levels in the culture medium (**Fig. 8a**,**b**). These results suggest that NRDc potentiates TACE-mediated NRG1 cleavage at the cell surface, whereas NRDc enhances BACE1 cleavage of NRG1 in intracellular compartments. Because the enhancement of BACE1-mediated cleavage of NRG1 was not associated with an increase in NTF levels in the culture medium, NRDc is thought to potentiate BACE1 in endocytic pathways and direct the cleaved NRG1 to degradation[31]. Similar to the direct interaction of NRDc and TACE[19], co-precipitation demonstrated that NRDc forms as trimolecular complex with BACE1 and NRG1, suggesting that these proteins physically and functionally interact (**Fig. 8c**).

Given these findings, we examined the expression pattern of endogenous NRG1 protein in fibroblasts derived from *Nrd1*$^{-/-}$ and *Nrd1*$^{+/+}$ mice. Western blot analysis using an antibody to the C terminus of NRG1 (NRG-C), which recognizes both full-length NRG1 and the C-terminal fragment of NRG1 (CTF), revealed an increase in full-length NRG1 and a decrease in CTF in *Nrd1*$^{-/-}$ cells compared with *Nrd1*$^{+/+}$ cells (**Fig. 8d**). In addition, although an antibody to the intracellular N terminus of NRG1 type III detected the cleaved NTF of NRG1 type III in *Nrd1*$^{+/+}$ cells, it barely detected the cleaved fragment in *Nrd1*$^{-/-}$ cells (**Fig. 8d**). These results indicate that NRDc positively regulates the proteolytic cleavage of both type I and type III NRG1.

Next, we examined the expression of NRG1 in brain extracts from *Nrd1*$^{+/+}$ and *Nrd1*$^{-/-}$ mice at P14. Western blotting with antibodies to the C terminus of NRG1 type I and the N terminus of NRG1 type III revealed a similar pattern as found in MEFs (**Fig. 8e**), although the difference between the two genotypes was less evident in the brain extract. These results are consistent with the fact that the proteolytic cleavage of NRG1 type I and type III in brain is regulated by NRDc. We then analyzed the protein expression of BACE1. The molecular

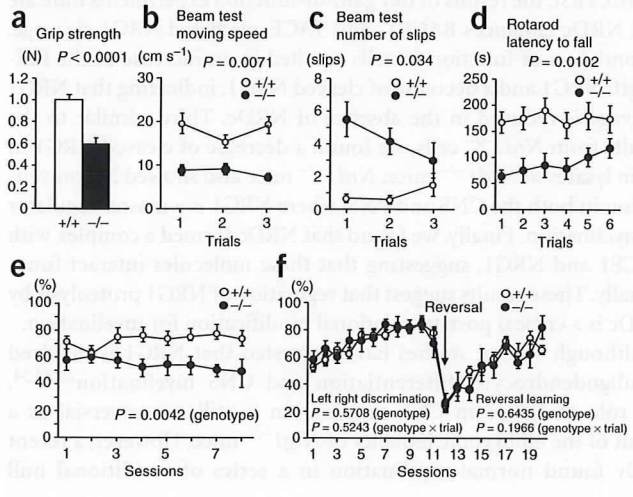

Figure 7 Impaired motor activity and cognitive deficits in *Nrd1*$^{-/-}$ mice. Mice at the age of 90–180 d were analyzed with a battery of behavioral tests (age-matched littermates; *Nrd1*$^{+/+}$, $n = 12$; *Nrd1*$^{-/-}$, $n = 6$). (**a**) Grip-strength test, measured in newtons. *Nrd1*$^{-/-}$ mice had reduced forelimb grip strength. (**b**,**c**) The ability of mice to traverse a narrow beam to reach a dark box was analyzed in a beam test. *Nrd1*$^{-/-}$ mice moved slower (**b**) and slipped more frequently (**c**) than *Nrd1*$^{+/+}$ mice. (**d**) Latency to fall from a rotating drum was measured in a rotarod test. *Nrd1*$^{-/-}$ mice had a shorter latency to fall. (**e**) The percentages of correct choices in the T maze forced-alteration task are shown. showing *Nrd1*$^{-/-}$ mice had impaired working memory. (**f**) The percentages of correct choices in the T maze left right–discrimination task are shown. There was no difference between *Nrd1*$^{+/+}$ and *Nrd1*$^{-/-}$ mice. The genotype effect was analyzed by a two-way repeated ANOVA in all tests. Data represent the mean ± s.e.m.

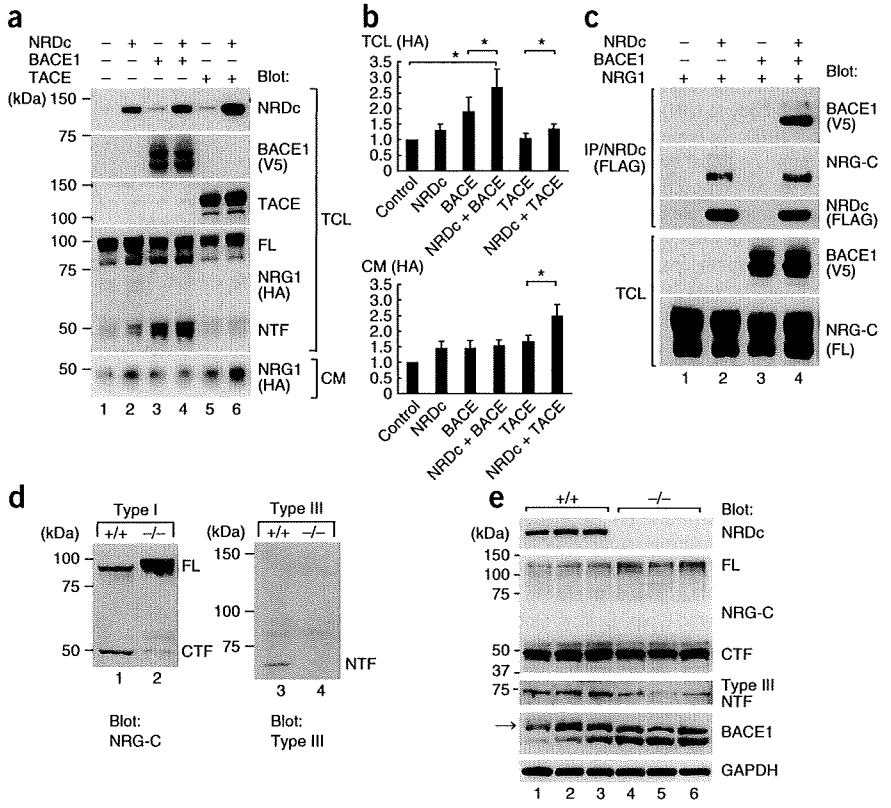

Figure 8 NRDc regulates NRG1 shedding through BACE1 and TACE. (**a**) FLAG-tagged NRDc, V5-tagged BACE1, TACE and HA-tagged NRG1 type I were coexpressed in COS7 cells. Immunoblot analyses with the indicated antibodies were performed. Note that the cleaved NTF of NRG1 in the total cell lysates (TCL) was increased by the addition of NRDc to BACE1 (lanes 3 and 4), whereas coexpression of NRDc with TACE clearly increased the NTF in the culture medium (CM) (lanes 5 and 6). (**b**) Quantification of the cleaved NTF in the TCL and culture medium by densitometry. The ratio was arbitrarily set at 1 in control vector–transfected cells. Data represent the mean ± s.e.m. in five independent experiments. * $P < 0.05$. (**c**) Immunoprecipitation of the co-transfected cell lysate with an antibody to FLAG reveled a complex of NRDc, BACE1 and NRG1. Only the full length (FL) of NRG1 is shown here. (**d**) Expression of endogenous NRG1 type I and NRG1 type III in MEFs isolated from *Nrd1*$^{+/+}$ or *Nrd1*$^{-/-}$ mice. Note that the full-length of NRG1 type I was increased and the cleaved CTF was decreased in *Nrd1*$^{-/-}$ cells (lane 2) and that the cleaved NTF of NRG1 type III was decreased in *Nrd1*$^{-/-}$ cells (lane 4). (**e**) Immunoblot analysis of brain extracts from control wild-type (+/+) and *Nrd1*$^{-/-}$ (−/−) mice at P14 ($n = 3$ in each genotype) with indicated antibodies. Note that the full length of NRG1 (~140 kDa) was increased, whereas the NTF of NRG1 type III (75 kDa) was decreased in *Nrd1*$^{-/-}$ brains. The mature form of BACE1 in *Nrd1*$^{+/+}$ brain extracts is indicated by an arrow. The ratio of the mature form to immature form was higher in *Nrd1*$^{+/+}$ than in *Nrd1*$^{-/-}$ brains.

size of mature BACE1 in *Nrd1*$^{-/-}$ brain was a little smaller than that in the *Nrd1*$^{+/+}$ brain (**Fig. 8e**). In addition, the ratio of the mature form to immature form of BACE1 was clearly higher in *Nrd1*$^{+/+}$ brains than in *Nrd1*$^{-/-}$ brains (*Nrd1*$^{+/+}$, 2.21 ± 0.62; *Nrd1*$^{-/-}$, 0.75 ± 0.08; $n = 3$, $P = 0.04$), indicating that the protein maturation of BACE1 was impaired in *Nrd1*$^{-/-}$ brains. These results suggest that NRDc regulates BACE1-mediated NRG1 shedding by affecting BACE1 maturation and BACE1 sheddase activity. On the other hand, the mRNA levels of *Nrg1* and *Bace1* were not different between *Nrd1*$^{+/+}$ and *Nrd1*$^{-/-}$ brains (**Supplementary Fig. 8**), indicating that NRDc post-translationally modulates the expression and activity of NRG1 and BACE1.

DISCUSSION

Our findings provide, to the best of our knowledge, the first *in vivo* evidence that NRDc is a critical regulator of axonal maturation and myelination in the CNS and PNS. In the CNS, axon diameter and myelin thickness correlated with levels of NRDc expression (homozygous < heterozygous < wild-type mice). Our results suggest that NRDc affects myelination by regulating axonal maturation, as myelin thickness is proportional to the diameter of axons[1,2]. Neuron-specific overexpression of NRDc, however, did not affect the axon caliber, but instead induced hypermyelination, providing additional evidence that NRDc is a critical regulator of myelination. Notably, as we did not see any differences in the number of oligodendrocyte precursor cells and the expression levels of specific oligodendrocyte precursor markers between *Nrd1*$^{+/+}$ and *Nrd1*$^{-/-}$ mice, NRDc appears to specifically regulate myelination and not oligodendrocyte differentiation or proliferation. In addition, as expression of NRDc is confined to neurons, the effect of NRDc on oligodendrocyte is non–cell autonomous. Instead, our data suggest that NRDc affects axonal signaling between neurons and oligodendrocytes.

NRG1 is the best-characterized neuronal factor that induces axonal signaling required for the entire program of glial differentiation, proliferation and myelination[8,10,32]. NRG1 is synthesized as a transmembrane protein that is proteolytically cleaved in the juxtamembrane region. ADAM proteases (TACE/ADAM17 (ref. 11) and ADAM19 (refs. 12,33)) and BACE1 (refs. 13,14) have been proposed to cleave NRG1. Furthermore, *Bace1*$^{-/-}$ mice exhibit hypomyelination[13–15] and *Adam19*$^{-/-}$ mice have delayed remyelination after injury[33], suggesting that proteolytic cleavage of NRG1 is important for myelination. Our data indicate that NRDc is a critical regulator of NRG1 cleavage *in vivo*. First, the results of our gain-of-function experiments indicate that NRDc enhances BACE1- and TACE-mediated NRG1 cleavage. Second, loss of function in cells resulted in an increase of the full-length NRG1 and a decrease of cleaved NRG1, indicating that NRG1 cleavage is reduced in the absence of NRDc. Third, similar to the results from *Nrd1*$^{-/-}$ cells, we found a decrease of cleaved NRG1 in brain lysates of *Nrd1*$^{-/-}$ mice. *Nrd1*$^{-/-}$ mice also showed hypomyelination in both the CNS and PNS, where NRG1 is a master regulator of myelination. Finally, we found that NRDc formed a complex with BACE1 and NRG1, suggesting that these molecules interact functionally. These results suggest that regulation of NRG1 proteolysis by NRDc is a critical post-translational modification for myelination.

Although several studies have suggested that NRG1 is involved in oligodendrocyte differentiation and CNS myelination[25,32,34], the role of NRG1 in CNS myelination is still controversial as a result of the embryonic lethality of *Nrg1*$^{-/-}$ mice. However, a recent study found normal myelination in a series of conditional null

mutants of *Nrg1* that lack the gene at different stages during CNS development, suggesting that NRG1 may function differently in the PNS and CNS[35]. Because our data indicate that NRDc regulates myelination in both the CNS and PNS, NRDc may affect different proteins in the CNS. On the other hand, although both *Nrd1*$^{-/-}$ and *Bace1*$^{-/-}$ mice had hypomyelination in the CNS and PNS, no abnormalities in axon diameter and initiation of myelination have been reported in *BACE1*$^{-/-}$ mice[13–15]. Taken together, the effect of NRDc in the CNS cannot be attributed merely to NRG1 or BACE1. We have previously shown that NRDc potentiates several ADAM proteases[19–21] and here we found that NRDc also enhanced the capacity of BACE1 to process NRG1. The enhancing effect of NRDc on ADAM proteases is not substrate-specific, as NRDc can potentiate TACE-mediated shedding of HB-EGF, TNF-α, APP and NRG1 (refs. 19–21). This might also be the case for BACE1, as we found that NRDc affects the maturation of BACE1 (**Fig. 8**).

Axonal maturation and myelination are essential in nerve conduction and aberrant in various neuropathologies. For example, the primary pathologic event of multiple sclerosis is demyelination and remyelination correlates with recovery from clinical symptoms[36]. Given the dose-dependent effect of NRDc on myelin thickness, NRDc could be a potential pharmacological target of this common neurological disorder of young adults. NRDc could also be important for the regeneration of injured axons. In fact, the critical regulatory functions of NRDc in axon-oligodendrocyte signaling, axon maturation and myelination suggest that NRDc may impinge on a broad range of neurological disorders.

METHODS

Methods and any associated references are available in the online version of the paper at http://www.nature.com/natureneuroscience/.

Note: Supplementary information is available on the Nature Neuroscience website.

ACKNOWLEDGMENTS

We are grateful to N. Nishimoto and H. Nakabayashi for technical assistance, and K. Matsumoto, E. Kimura, A. Kinoshita and A. Sehara for materials. We thank P.W. Park, T. Nishio, H. Fujiwara, T. Kaneko, F. Fujiyama and H. Kawasaki for critical reading of the manuscript. This study was supported by research grants (19041035, 20390255, 20659061, 20200068 and IBR-shien) from the Ministry of Education, Culture, Sports, Science and Technology of Japan. It was also supported by the Takeda Science Foundation, the Mochida Memorial Foundation for Medical and Pharmaceutical Research, the Suzuken Memorial Foundation, the Japan Health Foundation and the Daiichi Sankyo Sponsored Research Program.

AUTHOR CONTRIBUTIONS

M.O. and E.N. planned the experiments and wrote the manuscript. M.O., Y.H., T.M. and E.N. performed the experiments. H.T. carried out the histological procedures. K.T. and T.M. performed behavioral analysis. N.O. and H.K. generated the *Nrd1*$^{-/-}$ mice. T. Kimura and T. Kita supervised the work.

Published online at http://www.nature.com/natureneuroscience/.
Reprints and permissions information is available online at http://www.nature.com/reprintsandpermissions/.

1. Nave, K.A. & Trapp, B.D. Axon-glial signaling and the glial support of axon function. *Annu. Rev. Neurosci.* **31**, 535–561 (2008).
2. Simons, M. & Trotter, J. Wrapping it up: the cell biology of myelination. *Curr. Opin. Neurobiol.* **17**, 533–540 (2007).
3. Hartline, D.K. & Colman, D.R. Rapid conduction and the evolution of giant axons and myelinated fibers. *Curr. Biol.* **17**, R29–R35 (2007).
4. McTigue, D.M. & Tripathi, R.B. The life, death, and replacement of oligodendrocytes in the adult CNS. *J. Neurochem.* **107**, 1–19 (2008).
5. Griffiths, I. *et al.* Axonal swellings and degeneration in mice lacking the major proteolipid of myelin. *Science* **280**, 1610–1613 (1998).
6. Lappe-Siefke, C. *et al.* Disruption of Cnp1 uncouples oligodendroglial functions in axonal support and myelination. *Nat. Genet.* **33**, 366–374 (2003).
7. Michailov, G.V. *et al.* Axonal neuregulin-1 regulates myelin sheath thickness. *Science* **304**, 700–703 (2004).
8. Nave, K.A. & Salzer, J.L. Axonal regulation of myelination by neuregulin 1. *Curr. Opin. Neurobiol.* **16**, 492–500 (2006).
9. Mei, L. & Xiong, W.C. Neuregulin 1 in neural development, synaptic plasticity and schizophrenia. *Nat. Rev. Neurosci.* **9**, 437–452 (2008).
10. Falls, D.L. Neuregulins: functions, forms and signaling strategies. *Exp. Cell Res.* **284**, 14–30 (2003).
11. Montero, J.C., Yuste, L., Diaz-Rodriguez, E., Esparis-Ogando, A. & Pandiella, A. Differential shedding of transmembrane neuregulin isoforms by the tumor necrosis factor alpha–converting enzyme. *Mol. Cell. Neurosci.* **16**, 631–648 (2000).
12. Shirakabe, K., Wakatsuki, S., Kurisaki, T. & Fujisawa-Sehara, A. Roles of Meltrin beta/ADAM19 in the processing of neuregulin. *J. Biol. Chem.* **276**, 9352–9358 (2001).
13. Willem, M. *et al.* Control of peripheral nerve myelination by the beta-secretase BACE1. *Science* **314**, 664–666 (2006).
14. Hu, X. *et al.* Bace1 modulates myelination in the central and peripheral nervous system. *Nat. Neurosci.* **9**, 1520–1525 (2006).
15. Hu, X. *et al.* Genetic deletion of BACE1 in mice affects remyelination of sciatic nerves. *FASEB J.* **22**, 2970–2980 (2008).
16. Pierotti, A.R. *et al.* N-arginine dibasic convertase, a metalloendopeptidase as a prototype of a class of processing enzymes. *Proc. Natl. Acad. Sci. USA* **91**, 6078–6082 (1994).
17. Chesneau, V. *et al.* N-arginine dibasic convertase (NRD convertase): a newcomer to the family of processing endopeptidases. An overview. *Biochimie* **76**, 234–240 (1994).
18. Nishi, E., Prat, A., Hospital, V., Elenius, K. & Klagsbrun, M. N-arginine dibasic convertase is a specific receptor for heparin-binding EGF-like growth factor that mediates cell migration. *EMBO J.* **20**, 3342–3350 (2001).
19. Nishi, E., Hiraoka, Y., Yoshida, K., Okawa, K. & Kita, T. Nardilysin enhances ectodomain shedding of heparin-binding epidermal growth factor–like growth factor through activation of tumor necrosis factor alpha–converting enzyme. *J. Biol. Chem.* **281**, 31164–31172 (2006).
20. Hiraoka, Y. *et al.* Enhancement of alpha-secretase cleavage of amyloid precursor protein by a metalloendopeptidase nardilysin. *J. Neurochem.* **102**, 1595–1605 (2007).
21. Hiraoka, Y. *et al.* Ectodomain shedding of TNF-alpha is enhanced by nardilysin via activation of ADAM proteases. *Biochem. Biophys. Res. Commun.* **370**, 154–158 (2008).
22. Bernstein, H.G. *et al.* Histochemical evidence for wide expression of the metalloendopeptidase nardilysin in human brain neurons. *Neuroscience* **146**, 1513–1523 (2007).
23. Lu, Q.R. *et al.* Common developmental requirement for Olig function indicates a motor neuron/oligodendrocyte connection. *Cell* **109**, 75–86 (2002).
24. Fields, R.D. & Ellisman, M.H. Axons regenerated through silicone tube splices. II. Functional morphology. *Exp. Neurol.* **92**, 61–74 (1986).
25. Taveggia, C. *et al.* Neuregulin-1 type III determines the ensheathment fate of axons. *Neuron* **47**, 681–694 (2005).
26. Mayford, M., Wang, J., Kandel, E.R. & O'Dell, T.J. CaMKII regulates the frequency-response function of hippocampal synapses for the production of both LTD and LTP. *Cell* **81**, 891–904 (1995).
27. Dragatsis, I. & Zeitlin, S. CaMKIIalpha-Cre transgene expression and recombination patterns in the mouse brain. *Genesis* **26**, 133–135 (2000).
28. Yamasaki, N. *et al.* Alpha-CaMKII deficiency causes immature dentate gyrus, a novel candidate endophenotype of psychiatric disorders. *Mol Brain* **1**, 6 (2008).
29. Carter, R.J. *et al.* Characterization of progressive motor deficits in mice transgenic for the human Huntington's disease mutation. *J. Neurosci.* **19**, 3248–3257 (1999).
30. Takao, K. *et al.* Impaired long-term memory retention and working memory in sdy mutant mice with a deletion in Dtnbp1, a susceptibility gene for schizophrenia. *Mol Brain* **1**, 11 (2008).
31. Thinakaran, G. & Koo, E.H. Amyloid precursor protein trafficking, processing and function. *J. Biol. Chem.* **283**, 29615–29619 (2008).
32. Calaora, V. *et al.* Neuregulin signaling regulates neural precursor growth and the generation of oligodendrocytes *in vitro*. *J. Neurosci.* **21**, 4740–4751 (2001).
33. Wakatsuki, S., Yumoto, N., Komatsu, K., Araki, T. & Sehara-Fujisawa, A. Roles of meltrin-beta/ADAM19 in progression of Schwann cell differentiation and myelination during sciatic nerve regeneration. *J. Biol. Chem.* **284**, 2957–2966 (2009).
34. Taveggia, C. *et al.* Type III neuregulin-1 promotes oligodendrocyte myelination. *Glia* **56**, 284–293 (2008).
35. Brinkmann, B.G. *et al.* Neuregulin-1/ErbB signaling serves distinct functions in myelination of the peripheral and central nervous system. *Neuron* **59**, 581–595 (2008).
36. Trapp, B.D. & Nave, K.A. Multiple sclerosis: an immune or neurodegenerative disorder? *Annu. Rev. Neurosci.* **31**, 247–269 (2008).

Papers in Press. Published January 14, 2010 as doi:10.1373/clinchem.2009.140202
The latest version is at http://www.clinchem.org/cgi/doi/10.1373/clinchem.2009.140202

Clinical Chemistry 56:3
000–000 (2010)

Brief Communications

C-Reactive Protein Uptake by Macrophage Cell Line via Class-A Scavenger Receptor

Yoshiko Fujita, Akemi Kakino, Mariko Harada-Shiba, Yuko Sato, Kazunori Otsui, Ryo Yoshimoto, and Tatsuya Sawamura*

Department of Vascular Physiology, National Cardiovascular Center Research Institute, Suita, Osaka, Japan; *address correspondence to this author at: Department of Vascular Physiology, National Cardiovascular Center Research Institute, 5-7-1 Fujishirodai, Suita, Osaka 565-8565, Japan. Fax +81–6-6835–5329; e-mail t-sawamura@umin.ac.jp.

BACKGROUND: C-reactive protein (CRP) increases in response to inflammation and is purported to be a risk factor for atherogenesis. We recently demonstrated that a scavenger receptor, lectin-like oxidized LDL receptor (LOX-1), is a receptor for CRP. In light of the overlapping ligand spectrum of scavenger receptors such as modified LDL, bacteria, and advanced glycation end products, we examined whether other scavenger receptors recognize CRP.

METHODS: We analyzed the uptake of fluorescently labeled CRP in COS-7 cells expressing a series of scavenger receptors and in a monocytic cell line, THP-1, differentiated into macrophage with phorbol 12-myristate 13-acetate (PMA). We applied small interfering RNA (siRNA) against class-A scavenger receptor (SR-A) to THP-1 cells to suppress the expression of SR-A. We also analyzed the binding of nonlabeled CRP to immobilized recombinant LOX-1 and SR-A in vitro using anti-CRP antibody.

RESULTS: COS-7 cells expressing LOX-1 and SR-A internalized fluorescently labeled CRP in a dose-dependent manner, but cells expressing CD36, SR-BI, or CD68 did not. The recombinant LOX-1 and SR-A proteins recognized nonlabeled purified CRP and native CRP in serum in vitro. THP-1 cells differentiated into macrophage-like cells by treatment with PMA-internalized fluorescently labeled CRP. siRNA against SR-A significantly and concomitantly inhibited the expression of SR-A ($P < 0.01$) and CRP uptake ($P < 0.01$), whereas control siRNA did not.

CONCLUSIONS: CRP is recognized by SR-A as well as LOX-1 and taken up via SR-A in a macrophage-like cell line. This process might be of significance in the pathogenesis of atherosclerotic disease.

C-reactive protein (CRP),[1] which is synthesized by hepatocytes in response to inflammation and tissue damage *(1)*, binds to various ligands exposed on damaged tissues or bacteria promoting phagocytosis and complement activation with C1q *(1, 2)*. Plasma CRP concentrations may rise as much as 1000-fold during infection or inflammation *(3)*. In addition, CRP concentrations, within the reference range, can predict cardiovascular diseases *(4, 5)*, and there is a good correlation between plasma CRP concentrations and the degree of atherosclerosis in hypercholesterolemic rabbits *(6)*.

Fcγ receptors CD16, CD32, and CD64 have been reported as the receptors for CRP *(7–9)*. In addition, we recently demonstrated that CRP increases vascular permeability through a direct binding to lectin-like oxidized LDL receptor (LOX-1), which is expressed in endothelial cells *(10)*. Members of the scavenger receptor family, such as class A scavenger receptor (SR-A), CD36, LOX-1, and scavenger receptor B-I (SR-BI), recognize common ligands such as modified LDL, bacteria, and advanced glycation end products, and they are thought to affect the progression of atherosclerosis *(11, 12)*. In this study, to further elucidate the atherogenic properties of CRP, we addressed whether other scavenger receptors are involved in the recognition of CRP.

Human sera with high and normal concentrations of CRP were obtained from Dako. Human CRP purified from pleural fluid was purchased from Chemicon (AG723). Sodium azide in the solution was extensively removed by dialyzing 3 times against a 3000-fold volume of Dulbecco's PBS (Wako). Gram-negative bacterial endotoxins were undetectable by limulus amebocyte lysate (Associates of Cape Cod), which can detect as little as 0.03 endotoxin units per mL endotoxins. CRP was fluorescently labeled with CypHer5E (GE Healthcare) and dialyzed 3 times against a 3000-fold volume of PBS.

COS-7 cells maintained with Dulbecco's modified Eagle's medium (DMEM; Invitrogen)/10% fetal bovine serum (FBS) were seeded 1 day before transfection. After reaching 80%–90% confluency, we transfected the cells with the plasmid using Lipofectamin 2000 transfection reagent (Invitrogen). We used the following cDNAs: human LOX-1 (GenBank NM002543), SR-A (GenBank NM002445), CD36 (GenBank NM000072), SR-BI (GenBank NM005505), CD68 (GenBank NM001251), and

[1] Nonstandard abbreviations: CRP, C-reactive protein; LOX-1, lectin-like oxidized LDL receptor; SR, scavenger receptor; DMEM, Dulbecco's modified Eagle's medium; FBS, fetal bovine serum; siRNA, small interfering RNA; PMA, phorbol 12-myristate 13-acetate; SRA-C6, anti–SR-A antibody; DAPI, 4′,6-diamidino-2-phenylindole.

dectin-1 (GenBank NM197947), which were subcloned into pcDNA6.2/V5/GW/D-TOPO expression vector (Invitrogen). We used pcDNA3.1/V5-His/lacZ (Invitrogen) as a control. After 48 h, we washed the cells with DMEM:1% antibiotics and antimycotic (AbAm; Invitrogen). We replaced the medium with CypHer5E-CRP-containing DMEM/1% AbAm and incubated the cells for 2 h at 37 °C. After washing with PBS, the cells were fixed with phosphate-buffered formalin (Wako) and permeabilized with 0.1% Triton X-100/PBS. We detected the expression of each receptor by immunostaining with anti-V5 antibody (Nacalai Tesque) combined with Alexa 488 antimouse IgG (Invitrogen). The nuclei of the cells were counterstained with 0.5 mg/L 4′,6-diamidino-2-phenylindole (DAPI) (Sigma). We divided the fluorescence intensities of CypHer5E and Alexa 488 by the cell number in a field, then divided the CypHer5E-CRP fluorescence intensity in the field by the Alexa 488 fluorescence value. These quantitative analyses were performed with an IN Cell Analyzer 1000 system (GE Healthcare).

We prepared recombinant human SR-A (amino acids 76–358) as described for LOX-1 *(10)*. Recombinant human SR-A (0.1 μg) or BSA (0.1 μg, Sigma) was immobilized to each well of 384-well plates (High Bind; Corning) by incubating at 4 °C in PBS overnight. After 2 washes with PBS, the plates were blocked with 80 μL of 20% ImmunoBlock (DS Pharma)/PBS at 4 °C for 8 h. After washing twice with PBS, we added CRP in the reaction buffer (10 mmol/L HEPES, 150 mmol/L NaCl, 2 mmol/L $CaCl_2$, 1% BSA, pH 7.0) to each well and incubated them at 4 °C overnight. We detected the binding of CRP with a TMB Peroxidase EIA Substrate kit (Bio-Rad) as described for LOX-1 *(10)*. We obtained small interfering RNA (siRNA) duplex oligoribonucleotides targeting the SR-A coding region (GenBank NM002445) from Invitrogen and used stealth RNAi duplex (Invitrogen) as a negative control. The siRNA sequences were as follows: 5′-GAUAUAACUCAAAGUCUCACGGGAA-3′, 5′-UUCCCGUGAGACUUUGAGUUAUAUC-3′ and 5′-CAGACCUUGAGAAAUAUCACUUUAA-3′, 5′-UUAAAGUGAUAUUUCUCAAGGUCUG-3′.

THP-1 cells were maintained with 10% FBS/1% AbAm/20 μmol/L mercaptoethanol:RPMI 1640 and differentiated with 100 nmol/L phorbol 12-myristate 13-acetate (PMA) (Sigma) for 48 h. We transfected the cells with siRNA oligos or control siRNA using Lipofectamin 2000 transfection reagent (Invitrogen) according to the manufacturer's instruction. After incubation at 37 °C for 24 h, we washed the cells with RPMI 1640/1% AbAm and replaced the medium with CypHer5E-CRP–containing RPMI 1640/1% AbAm, and the cells were incubated for 2 h. After washing with PBS, the cells were fixed with phosphate-buffered formalin (Wako) and permeabilized with 0.1% Triton X-100/PBS. We detected the effects of downregulation of SR-A gene expression by immunostaining with anti–SR-A antibody (SRA-C6; Trans Genic Inc) combined with Alexa 488 antimouse IgG. For detection of Fcγ receptors, we used anti-CD32 antibody (AT10; Santa Cruz) and anti-CD64 antibody (10.1; Santa Cruz). For CRP detection, we used anti-CRP antibody (Bethyl). The nuclei of the cells were counterstained with 0.5 mg/L DAPI. We divided the fluorescence intensities of CypHer5E and Alexa 488 by the cell number in a field. Quantitative analysis was performed with an IN Cell Analyzer 1000 system. All transfections were performed in triplicate.

All data are presented as mean (SE). Statistical analysis was performed with Student *t*-test. A P value <0.05 was considered statistically significant.

We examined whether CRP binds to scavenger receptors: LOX-1, SR-A, CD36, SR-BI, CD68, and dectin-1. Dectin-1 has the closest structural similarity to LOX-1 and belongs to C-type lectin-like molecule, although it is not a member of scavenger receptors.

Alexa546-labeled CRP at the concentration of 1 mg/L at 4 °C bound significantly to LOX-1–expressing cells ($P < 0.01$) but bound poorly to the cells expressing the other receptors (Supplemental Fig. 1, which accompanies the online version of this article at www.clinchem.org/content/vol56/issue3). Cellular uptake of CypHer5E-labeled CRP, which shows fluorescence after endocytosis, was significantly higher in SR-A–expressing cells, in a dose-dependent manner (1–30 mg/L), as well as in LOX-1–expressing cells, compared with cells expressing the other receptors (Fig. 1). Immunostaining with anti-V5 antibody revealed that all the receptors were expressed at a similar level in the respective cells.

Using anti-CRP antibody, we confirmed that nonlabeled CRP was also taken up by SR-A–expressing COS-7 cells. We further observed a significant binding of nonlabeled CRP (0.1–1 mg/L) to immobilized recombinant SR-A ($P < 0.01$) (online Supplemental Fig. 2). The binding was not affected by polymyxin B (5 mg/L), suggesting that it did not depend on the presence of endotoxin. Importantly, native CRP contained in human serum showed significant binding to SR-A, as well as to LOX-1 ($P < 0.01$) (online Supplemental Fig. 3). The binding was dependent on the concentration of CRP in the serum, suggesting that SR-A and LOX-1 have a capacity to bind to a native form of CRP in serum in the presence of other plasma proteins. These results indicate that SR-A and LOX-1 are the receptors for CRP among the examined receptors.

Because SR-A works in the monocyte-macrophage system, we assessed whether CRP is taken up by macrophages via SR-A. We used a human monocytic cell line,

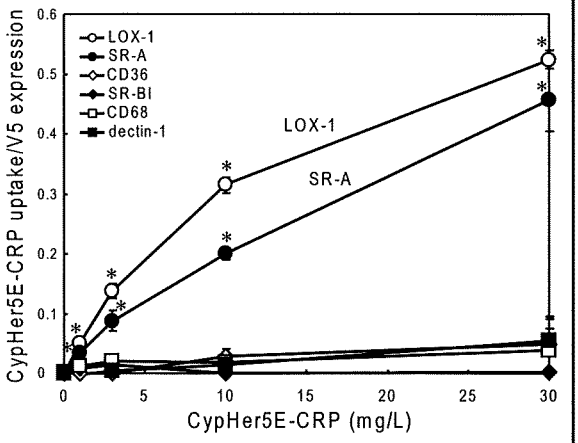

Fig. 1. Quantitative analyses of CypHer5E-CRP taken up by COS-7 cells expressing LOX-1, SR-A, CD36, SR-BI, and dectin-1.

Signals observed in the cells transfected with pcDNA3.1/V5-His/lacZ were considered as non-specific background. *Significant difference vs. negative control ($P < 0.01$).

THP-1, after inducing differentiation into macrophage by the treatment of PMA *(13)*. In PMA-treated THP-1 cells, CypHer5E-CRP was taken up in a dose-dependent manner (0.3–30 mg/L). SR-A expression and CRP uptake were concomitantly suppressed by 2 different siRNAs targeting SR-A, but not by control siRNA (Table 1). The siRNA targeting SR-A did not affect the expression of Fcγ receptors (data not shown), indicating that CRP is taken up mainly via SR-A in a macrophage cell line, at least under these conditions.

The ligand specificity of the scavenger receptor family overlaps considerably *(11, 12)*, and while all can bind to oxidized LDL, only SR-A or LOX-1 bound to CRP. Interestingly, dectin-1, the most structurally similar molecule to LOX-1, did not bind to CRP.

Using a monoclonal antibody, a previous report suggested the presence of an unknown receptor other than Fcγ receptors in macrophages *(14)*. It has been reported that fucoidin, a ligand for SR-A, inhibits the in vivo CRP-promoted uptake of oxidized LDL *(15)*. SR-A might be the unidentified CRP receptor. Fcγ receptors and SR-A are under different regulation of gene expression. In fact, in response to differentiation stimulus of PMA, the expression of SR-A is strongly induced, whereas the expression of Fcγ receptors is suppressed *(16, 17)*. Conversely, stimulation by interferon-γ enhances the expression of Fcγ receptors but suppresses the expression of SR-A *(18)*. These results suggest that Fcγ receptors and SR-A would work in the cells stimulated by different molecules.

Table 1. Suppression of the uptake of fluorescently labeled CRP by siRNA against SR-A in differentiated THP-1 cells.[a]

siRNA	SR-A expression, %	CypHer5E-CRP, %
None	103 (3.2)	108 (9.1)
Control siRNA	100 (2.7)	100 (9.8)
siRNA1 for SR-A	17 (1.6)[b]	31 (3.9)[b]
siRNA2 for SR-A	13 (0.0)[b]	32 (1.1)[b]

[a] Data are as mean (SE).
[b] Significant difference vs control siRNA groups ($P < 0.01$).

Interestingly, the activity of SR-A as CRP receptor was more pronounced in the uptake of CRP, whereas LOX-1 showed strong activity in both binding and uptake. Because SR-A works in phagocytes, the CRP uptake activity of SR-A is reasonable. CRP was originally identified as a binding protein for bacterial component C-polysaccharide *(3)*. SR-A may function to engulf bacteria, viruses, and harmful substances opsonized by CRP in a context of innate immunity.

Related to epidemiological risk factors for cardiovascular disease, the presence of CRP in atheroma has been reported in both rabbits and humans *(6)*. Furthermore, the colocalization of CRP and SR-A in macrophages in atheromas has been reported *(19)*. Taking these reports together with the present results, SR-A-mediated CRP uptake by macrophages in atheromas might affect the foam cell formation and progression of atherosclerotic disease.

Author Contributions: *All authors confirmed they have contributed to the intellectual content of this paper and have met the following 3 requirements: (a) significant contributions to the conception and design, acquisition of data, or analysis and interpretation of data; (b) drafting or revising the article for intellectual content; and (c) final approval of the published article.*

Authors' Disclosures of Potential Conflicts of Interest: *Upon manuscript submission, all authors completed the Disclosures of Potential Conflict of Interest form. Potential conflicts of interest:*

Employment or Leadership: None declared.
Consultant or Advisory Role: None declared.
Stock Ownership: None declared.
Honoraria: None declared.
Research Funding: This study was supported in part by grants from the Ministry of Education, Culture, Sports, Science and Technology of Japan; the Ministry of Health, Labour and Welfare of Japan; the National Institute of Biomedical Innovation; and Japan Science and Technology Agency.
Expert Testimony: None declared.

Role of Sponsor: The funding organizations played no role in the design of study, choice of enrolled patients, review and interpretation of data, or preparation or approval of manuscript.

References

1. Black S, Kushner I, Samols D. C-reactive protein. J Biol Chem 2004;279:48487–90.
2. Volanakis JE, Kaplan MH. Interaction of C-reactive protein complexes with the complement system. II. Consumption of guinea pig complement by CRP complexes: requirement for human C1q. J Immunol 1974;113:9–17.
3. Gabay C, Kushner I. Acute-phase proteins and other systemic responses to inflammation. N Engl J Med 1999;340:448–54.
4. Ridker PM, Cushman M, Stampfer MJ, Tracy RP, Hennekens CH. Inflammation, aspirin, and the risk of cardiovascular disease in apparently healthy men. N Engl J Med 1997;336:973–9.
5. Ridker PM, Danielson E, Fonseca FA, Genest J, Gotto AM Jr, Kastelein JJ, et al. Rosuvastatin to prevent vascular events in men and women with elevated C-reactive protein. N Engl J Med 2008; 359:2195–207.
6. Sun H, Koike T, Ichikawa T, Hatakeyama K, Shiomi M, Zhang B, et al. C-reactive protein in atherosclerotic lesions: its origin and pathophysiological significance. Am J Pathol 2005;167: 1139–48.
7. Khreiss T, Jozsef L, Hossain S, Chan JS, Potempa LA, Filep JG. Loss of pentameric symmetry of C-reactive protein is associated with delayed apoptosis of human neutrophils. J Biol Chem 2002; 277:40775–81.
8. Bharadwaj D, Stein MP, Volzer M, Mold C, Du Clos TW. The major receptor for C-reactive protein on leukocytes is Fcgamma receptor II. J Exp Med 1999;190:585–90.
9. Stein MP, Mold C, Du Clos TW. C-reactive protein binding to murine leukocytes requires Fc gamma receptors. J Immunol 2000;164:1514–20.
10. Fujita Y, Kakino A, Nishimichi N, Yamaguchi S, Sato Y, Machida S, et al. Oxidized LDL receptor LOX-1 binds to C-reactive protein and mediates its vascular effects. Clin Chem 2009;55:285–94.
11. Moore KJ, Freeman MW. Scavenger receptors in atherosclerosis: beyond lipid uptake. Arterioscler Thromb Vasc Biol 2006;26:1702–11.
12. Greaves DR, Gordon S. The immune system and atherogenesis: recent insights into the biology of macrophage scavenger receptors. Thematic review series. J Lipid Res 2005;46:11–20.
13. Nishimura N, Harada-Shiba M, Tajima S, Sugano R, Yamamura T, Qiang QZ, Yamamoto A. Acquisition of secretion of transforming growth factor-beta 1 leads to autonomous suppression of scavenger receptor activity in a monocyte-macrophage cell line, THP-1. J Biol Chem 1998; 273:1562–7.
14. Tebo JM, Mortensen RF. Characterization and isolation of a C-reactive protein receptor from the human monocytic cell line U-937. J Immunol 1990;144:231–8.
15. Singh U, Dasu MR, Yancey PG, Afify A, Devaraj S, Jialal I. Human C-reactive protein promotes oxidized low density lipoprotein uptake and matrix metalloproteinase-9 release in Wistar rats. J Lipid Res 2008;49:1015–23.
16. Fleit HB, Kobasiuk CD. The human monocyte-like cell line THP-1 expresses Fc gamma RI and Fc gamma RII. J Leukoc Biol 1991;49:556–65.
17. Morganelli PM, Kennedy SM, Mitchell TI. Differential effects of interferon-gamma on metabolism of lipoprotein immune complexes mediated by specific human macrophage Fcgamma receptors. J Lipid Res 2000;41:405–15.
18. Geng YJ, Hansson GK. Interferon-gamma inhibits scavenger receptor expression and foam cell formation in human monocyte-derived macrophages. J Clin Invest 1992;89:1322–30.
19. Turk JR, Carroll JA, Laughlin MH, Thomas TR, Casati J, Bowles DK, Sturek M. C-reactive protein correlates with macrophage accumulation in coronary arteries of hypercholesterolemic pigs. J Appl Physiol 2003;95:1301–4.

Previously published online at
DOI: 10.1373/clinchem.2009.140202

LOX-1 mediates vascular lipid retention under hypertensive state

Atushi Nakano[a], Nobutaka Inoue[a], Yuko Sato[a], Norihisa Nishimichi[b], Kenji Takikawa[b], Yoshiko Fujita[a], Akemi Kakino[a], Kazunori Otsui[a], Saburo Yamaguchi[a], Haruo Matsuda[b] and Tatsuya Sawamura[a]

Objectives **Hypertension is a powerful independent risk factor for atherosclerotic cardiovascular diseases; however, the precise molecular mechanisms whereby hypertension promotes atherosclerotic formation remain to be determined. The interaction between oxidized low-density lipoprotein (oxLDL) and its receptor lectin-like oxidized low-density lipoprotein receptor-1 (LOX-1) plays a critical role in atherogenesis. To clarify how hypertension promotes atherosclerosis, we investigated specific roles of LOX-1 in acceleration of lipid deposition under a hypertensive state.**

Methods **We employed a model of stroke-prone spontaneously hypertensive rats (SHR-SP) that exhibits acute lipid deposition in mesenteric artery induced by high fat and salt loading. These vascular lipid deposition lesions share similar characteristics with the initial lesions of human atherosclerosis.**

Results **The enhanced LOX-1 expression in SHR-SP was associated with oxidized LDL deposited in vascular wall. Anti-LOX-1 neutralizing antibody dramatically suppressed the lipid deposition *in vivo* in SHR-SP. Vitamin E decreased serum oxLDL-like LOX-1 ligands, and suppressed the vascular lipid deposition. The vascular permeability, evaluated by the leakage of Evans blue, was markedly enhanced by pretreatment of oxLDL. The enhancement of vascular permeability induced by oxLDL was suppressed by anti-LOX-1 antibody.**

Conclusion **The enhanced expression and activation of LOX-1 mediated the enhancement of vascular permeability, which contributed to the vascular lipid accumulation under hypertensive states. *J Hypertens* 28:000–000 © 2010 Wolters Kluwer Health | Lippincott Williams & Wilkins.**

Journal of Hypertension 2010, 28:000–000

Keywords: LOX-1, oxidized low-density lipoproteins, SHR-SP

Abbreviations: ApoB, Apo-lipoprotein B; DiI, 1,1-dioctadecyl-3,3,3,3-tetramethylindocarbocyanine perchlorate; DiI-oxLDL, DiI-labeled oxLDL; GAPDH, glyceraldehyde 3-phosphate dehydrogenase; HDL, high-density lipoprotein; KRS, Krebs-Ringer solution; LDL, low-density lipoprotein; LOX-1, lectin-like oxidized low-density lipoprotein receptor-1; MBP, mean blood pressure; MFI, mean fluorescence intensity; oxLDL, oxidized low-density lipoprotein; PCR, polymerase chain reaction; SHR, spontaneously hypertensive rats; SHR-SP, stroke-prone spontaneously hypertensive rats; SMC, smooth muscle cells; TC, total cholesterol; Vit-E, Vitamin E; WKY, Wistar–Kyoto rats

[a]Department of Vascular Physiology, National Cardiovascular Center Research Institute, Fujishirodai, Suita, Osaka, Japan and [b]Laboratory of Immunobiology, Department of Molecular and Applied Biosciences, Graduate School of Biosphere Science, Hiroshima University, Hiroshima, Japan

Correspondence to Tatsuya Sawamura, MD, PhD, Director, Department of Vascular Physiology, National Cardiovascular Center Research Institute, 5-7-1, Fujishirodai, Suita, Osaka 565-8565, Japan
Tel: +81 6 6833 5012 x2518; fax: +81 6 6835 5329;
e-mail: t-sawamura@umin.ac.jp

Received 30 July 2009 **Revised** 28 December 2009
Accepted 1 February 2010

Introduction

An elevation of either systolic or diastolic pressure is a powerful independent risk factor for atherosclerotic cardiovascular diseases [1]. Yamori *et al.* [2] presented important findings, soon after the development of spontaneously hypertensive rats (SHR). Namely, SHR rapidly developed arterial lipid deposition in mesenteric artery and the basilar artery as well as a greater hypercholesterolemic response within two weeks when fed a high-fat diet and 1% salt loading in drinking water [2,3]. This rapid accumulation of lipids, which is referred to as acute atherosis, shares similar characteristics with fatty streak of the initial atherosclerotic lesion. This experimental model, therefore, is useful and appropriate for analyzing pharmacological effects of various substances on the process of atherosclerosis.

Since the proposal of 'the response to endothelial injury/dysfunction hypothesis' [4], the role of endothelial cells in the pathogenic mechanisms of atherosclerosis have been well recognized. On the contrary, 'the response-to-retention model' in early atherosclerosis [5,6] proposed that the retention of lipoprotein in the vessel wall is essential for atherogenesis. Indeed, it is reported that the above-mentioned fatty streak lesion can be found even in young children and infants. The lipid retention, so-called acute atherosis, is also well documented in the maternal vasculature of women with preeclampsia [7,8].

Lectin-like oxidized low-density lipoprotein receptor-1 (LOX-1) was identified as the receptor for oxidized low-density lipoprotein (oxLDL) on endothelial cells [9]. Since this discovery, accumulating evidence has

0263-6352 © 2010 Wolters Kluwer Health | Lippincott Williams & Wilkins DOI:10.1097/HJH.0b013e32833835d4

suggested that the atherogenic properties of oxLDL affecting endothelial cells are mediated mainly via LOX-1. OxLDL induces endothelial dysfunction/apoptosis, a major change in vascular biology observed at the beginning of atherogenesis through LOX-1-mediated pathway [10]. Furthermore, the binding of ligands to LOX-1 induces the activation of NADPH oxidase [11–13], which leads to oxidative stress in the vessel wall. LOX-1 is dynamically up-regulated by various atherogenic substances such as advanced glycated end products, angiotensin II, and oxLDL itself [14–16]. Furthermore, the expression of LOX-1 is enhanced under various proatherogenic conditions, such as diabetes, hypertension [17], and dyslipidemia [18–20]. Reflecting the proatherogenic properties of LOX-1, disruption of LOX-1 gene in mice actually preserved endothelial function and reduced atherogenesis under hyperlipidemia. Recently, Sankaralingam *et al.* [21] reported the enhanced expression of LOX-1 in association with the condition of preeclampsia.

In the present study, we sought to establish the role of LOX-1 in the arterial wall lipid deposition under hypertension, utilizing SHR-SP. Here, we present the experimental results, which link endothelial dysfunction and vascular lipid retention model via LOX-1.

Materials and methods

Animals

All protocols were approved by the Institutional Animal Care and Use Committee of the National Cardiovascular Center. Eight-week-old male SHR-SP and Wistar–Kyoto rats (WKY) (Japan SLC, Hamamatsu, Japan) were fed with high-fat chow (1.25% cholesterol, 0.5% cholate, 20% milk casein, 15% cocoa butter; α-tocopherol: 2 mg/kg chow) and physiological saline (9 g/l NaCl) instead of drinking water. To evaluate the involvement of LOX-1-mediated pathway, anti-LOX-1 antibody (TS20; 10 mg/kg body weight) or nonimmune mouse IgG (I5381; 10 mg/kg body weight, Sigma-Aldrich, St. Louis, Missouri, USA) was administered via a tail vein two times, just before and on the fourth day of a week's loading. TS20 is the antibody formerly named JTX20 [22]. To some animals indicated in the results, the high-fat diet supplemented with α-tocopherol (50 mg/kg chow) was fed. Body weight and blood pressure were measured before loading and every other day during the examination. Blood pressure was determined by a non-invasive tail cuff and pulse transducer system (BP-98A; Softron, Tokyo, Japan).

After the loading period, the rats were euthanized with inhalation of diethyl ether. The abdominal cavity was immediately opened, and a systemic venous blood was sampled from inferior vena cava. Then, the rat was perfused systemically with physiological saline solution. The mesentery was excised out with intestine. Then, the enteric canal and mesenteric fat and vein were removed to isolate mesenteric artery. Serum levels of total cholesterol (TC), triglyceride, phospholipids, and high-density lipoprotein (HDL) were determined using commercially available reagent kits (Wako, Tokyo, Japan).

Quantitative reverse transcription-polymerase chain reaction

Expression of LOX-1 mRNA in rat mesenteric artery was evaluated by quantitative reverse transcription–polymerase chain reaction (QRT-PCR). Complementary DNA was synthesized with total RNA (1 μg/ml per sample) and random hexamers using SuperScript III RNase H-reverse transcriptase (Invitrogen, Carlsbad, California, USA). Aliquots from each cDNA solution were subjected to QRT-PCR using a primer pair and a quencher specific to rat LOX-1 sequence (Rn00591116) using TaqMan Universal PCR Master Mix (Applied Biosystems, Foster City, California, USA). A GAPDH fragment was amplified as an internal control. Data are expressed as the ratio of LOX-1 to GAPDH mRNA.

Whole-mount immunohistochemistry

The segments of mesenteric artery were fixed with 2% formalin, and incubated consecutively with 1 mg/ml of dispase/PBS, 2% formalin/0.2% Triton X-100/PBS, methanol at −20°C, and 0.1% Triton X-100 in Tris-buffered saline. After blocking, the tissues were stained with Cy3-labeled antibovine LOX-1 antibody (TS20, 5 μg/ml) or Cy3-labeled mouse IgG as a negative control. The tissues were dehydrated in graded alcohols, and cleared in xylene. A whole-mount immunohistochemical image was obtained by a confocal laser microscope (Fluoview; Olympus, Tokyo Japan).

Oil Red O staining of accumulated lipid in mesenteric arteries

Oil Red O staining was used to detect lipid deposition in mesenteric arteries. The isolated mesenteric artery was fixed with 10% formalin, and washed with PBS. After flushing with 60% isopropanol for 5 min at room temperature, the blood vessel was incubated for 15 min at 55°C with 0.6% Oil Red O (Merck KGaA, Darmstadt, Germany) in 60% isopropanol. Then, the vessel was serially rinsed with 60 and 30% isopropanol, and PBS. The number of lipid deposits was manually counted under the stereomicroscope (Stemi 2000; Carl Zeiss, Göttingen, Germany).

Immunohistochemistry

Freshly frozen cross-sections of mesenteric artery were fixed with 10% formalin. The sections were incubated with 25% Block Ace (Dainippon Sumitomo Pharma, Osaka, Japan) and 5% donkey serum at 4°C overnight. The sections were incubated with anti-LOX-1 antibody (1 μg/ml, TS20), rabbit anti-oxLDL antiserum (1/100, AB3232; Chemicon, Temecula, California, USA), anti-smooth muscle actin (1 μg/ml, 1A4; DAKO, Carpinteria,